International Journal of Heat and Mass Transfer 170 (2021) 121022

Contents lists available at ScienceDirect

International Journal of Heat and Mass Transfer

journal homepage: www.elsevier.com/locate/hmt

Effects of the diffusive mixing and self-discharge reactions in microfluidic membraneless vanadium redox flow batteries

Santiago E. Ibáñez[a,c,*], Alberto E. Quintero[b], Pablo A. García-Salaberri[c], Marcos Vera[c]

[a] Electrochemical Processes Unit, IMDEA Energy Institute, Avda. Ramón de La Sagra 3, 28935, Móstoles, Spain
[b] Micro Electrochemical Technologies, Calle Federico Cantero Villamil, 2-B, 28935, Móstoles, Spain
[c] Departamento de Ingeniería Térmica y de Fluidos, Universidad Carlos III de Madrid, Av. de la Universidad 30, Leganés, 28911, Spain

ARTICLE INFO

Article history:
Received 6 August 2020
Revised 4 January 2021
Accepted 22 January 2021
Available online 6 February 2021

Keywords:
Vanadium redox flow battery
Membraneless
Crossover
Self-discharge reactions
Reaction fronts
Capacity fade

ABSTRACT

Microfluidic-based membraneless redox flow batteries have been recently proposed and tested with the aim of removing one of the most expensive and problematic components of the system, the ion-exchange membrane. In this promising design, the electrolytes are allowed to flow parallel to each other along microchannels, where they remain separated thanks to the laminar flow conditions prevailing at sub-millimeter scales, which prevent the convective mixing of both streams. The lack of membrane enhances proton transfer and simplifies overall system design at the expense of larger crossover rates of vanadium ions. The aim of this work is to provide estimates for the crossover rates induced by the combined action of active species diffusion and homogeneous self-discharge reactions. As the rate of these reactions is still uncertain, two limiting cases are addressed: infinitely slow (frozen chemistry) and infinitely fast (chemical equilibrium) reactions. These two limits provide lower and upper bounds for the crossover rates in microfluidic vanadium redox flow batteries, which can be conveniently expressed in terms of analytical or semi-analytical expressions. In summary, the analysis presented herein provides design guidelines to evaluate the capacity fade resulting from the combined effect of vanadium cross-over and self-discharge reactions in these emerging systems.

1. Introduction

During the last decades, it has become clear that the current dependence on fossil fuels as a primary energy source can not be sustained in the long term. The depletion of fossil reserves and the growing concerns about global warming will undoubtedly shift this paradigm to renewable energy sources, such as wind or solar. However, renewable energy sources are limited to intermittent periods of production [1,2]. Thus, widespread use of renewable energy sources will rely on the development of inexpensive energy storage solutions. Redox Flow Batteries (RFBs) are considered good candidates for stationary energy storage due to its longer lifetimes compared to, e.g., lithium-ion batteries. Another salient feature of RFBs is their ability to decouple power from energy, thus allowing designs that can be scaled-up in a more cost-effective manner due to the simplicity of the system [3].

Among all different chemical compounds that are used as active species in the electrolytes of RFBs, the all-vanadium redox couple is the most widely used. Both electrolytes of these batteries contains compounds of vanadium ions with different states of oxidation dissolved in concentrated sulphuric acid. Compatibility issues due to the mixing of both electrolytes are absent and the imbalances of vanadium ion concentrations are easily addressed by mixing both electrolytes and separating them into two equal parts.

Although RFBs were first developed in the70ʳs, nowadays there is a renewed interest on this technology. Recent advances in RFBs include the development of new active species other from the classical metal redox couples. Organic species, such as quinones [4], have attracted the attention of the community during the last years due to the cost reduction resulting from their greater availability compared to metal-based systems [5]. Improvements on the electrodes aiming to increase the specific reaction area and to enhance the electrical conductivity have also been achieved mainly with two approaches, surface treatments on the materials already present (as thermal activation and plasma treatment) [6,7], and deposition of electrocatalyst materials over the electrodes [8,9]. Even though vanadium RFBs (VRFBs) have been the most widely studied

* Corresponding author.
E-mail addresses: santiago.ibanez@imdea.org, sibanez@ing.uc3m.es (S.E. Ibáñez), alberto.quintero@b5tec.com (A.E. Quintero), pagsalab@ing.uc3m.es (P.A. García-Salaberri), marcos.vera@uc3m.es (M. Vera).

https://doi.org/10.1016/j.ijheatmasstransfer.2021.121022

Nomenclature

A	integration constant [mol m^{-3}]
B	integration constant [mol m^{-3}]
c_i	molar concentration of species i [mol m^{-3}]
C	integration constant [mol m^{-3}]
CR	inlet concentrations ratio [-]
d^+, d^-	reaction front position [m]
D	species diffusivity [m^2 s^{-1}]
Da	Damköler number [-]
F	Faraday constant [A s mol^{-1}]
H	half-channel height [m]
L	channel length [m]
n	species electric charge [-]
Pe	Peclet number [-]
P_l	stream-wise pressure gradient [kg m^{-2} s^{-2}]
Q	total volumetric flow rate [m^3 s]
R	universal gas constant [J mol^{-1} K^{-1}]
S	species chemical source term [mol m^{-3} s^{-1}]
SoC	state of charge of the electrolyte [-]
t	time [s]
T	temperature [K]
U	electrolyte velocity in the mixing region [m s^{-1}]
W	half-channel width [m]
z	passive scalar [mol m^{-3}]

Greek letters

α_i	crossover molar flux of species i per unit depth [mol m^{-1}s^{-1}]
α_i^{3D}	crossover molar flux of species i [mol s^{-1}]
γ	diffusivity ratio [-]
δ	mixing region thickness [m]
δ_R	reaction front thickness [m]
δ_w	mixing region thickness near walls [m]
κ	reaction constants [Depends on the kinetics]
ν	species mobility [mol s kg^{-1}]
Φ	electric potential [V]
Λ	channel aspect ratio W/H [-]
σ	electric conductivity [S m^{-1}]
Σ	reaction front
φ	species molar flux per unite depth lost by self-discharge reactions [mol m^{-1} s^{-1}]
ω	reaction rate [mol m^{-3} s^{-1}]
Ω	solution domains

Operators

Δ	delta operator, denotes change or difference
∇	nabla operator

Subscripts

i	species i
f	fast chemistry limit
s	slow chemistry limit

over time [10], there are still uncertainties related to active sites, reaction mechanisms, and reaction rates [11,12] among other aspects.

Applying microfluidic concepts to RFBs, stratified laminar co-flow cells are among the most disruptive advances introduced in the field during the last years [13–15]. The main advantage of micro-RFBs is that they do not require the membrane separator between the anolyte and the catholyte, an important contribution to the ohmic resistance in conventional designs. The membrane acts as a physical barrier that avoids the contact between the electrodes, but also as a selective barrier for active species that, ideally, allows only protons to travel from one electrolyte to the other to restore charge balance.

First attempts to develop Membraneless RFBs (MRFBs) are recent. Ferrigno et al. [15] tested the first prototype of a vanadium MRFB (VMRFB) with a single microchannel of rectangular cross section and planar electrodes at the bottom of the microchannel. Choban et al. [16] used a single microchannel geometry with planar electrodes on the walls to study the performance with formic acid and an oxidant agent, obtaining current densities up to 8 mA/cm^2. Innovative three dimensional architectures employing graphite rod electrodes or flow-through porous electrodes were introduced by Kjeang et al. [17,18]. Lee et al. [19] carried out a charge-discharge process in the first proof of concept of a VMRFB. A significant improvement of their design with respect to previous ones was the recollection of the anolyte and catholyte streams through separated ducts at the outlet of the microchannel, which allowed the operation of the VMRFB in continuous charge-discharge cycles. Goulet et al. [20] obtained power densities up to 2 W/cm^2 through an optimized design and using carbon nanotubes in the electrolyte solutions. Navalpotro et al. [21] reported an interesting attempt to build macroscale MRFBs based on immiscible redox electrolytes that could likely be extrapolated to micro-scale designs.

MRFB design has to deal with two competing ideas. One is the maximization of the amount of active species that can be charged in the electrodes and the other is the minimization of the charged species that cross and discharge in the opposite electrolyte. In practical applications, the selective transport of ions through the membrane is not perfect and crossover of active species is always present during RFB operations [22]. As a result, the battery presents a capacity fade over time. The microfluidic nature of MRFBs may help to overcome these problems through innovative cell and system designs [23]. On the other hand, flat electrodes have been optimized in order to increase the conversion rate of active species [24–28]. The problem of diffusive mixing between two parallel laminar co-flowing streams has been studied by Holl et al. [29] where they optimize microfluidic H-filters used to separate molecules or particles with different diffusion coefficients. One approach to limit the diffusive transport responsible of species crossover in MRFB is to reduce the contact area between the two fluid streams by using appropriate geometries for the flow cell [30].

Few investigations have addressed the rate of self-discharge reactions in VMRFBs. In most macro-scale models, these reactions are assumed to be instantaneous [31,32]. This is a good approximation in conventional designs where porous electrodes are in direct contact with the membrane, thereby enabling the fast conversion of the crossover species through heterogeneous reactions. As a result, the self-discharge rate is mass-transport limited by the presence of the membrane. By contrast, in micro-scale membraneless devices the electrodes do not interact with the mixing layer between the electrolytes, and the rates of the homogeneous self-discharge reactions play an important role in determining the capacity fade and efficiency of the micro battery.

Since the development of the first MRFB, different modeling studies have been carried out aiming to understand the flow behavior and to improve cell performance. Bazylak et al. [33] proposed a Computational Fluid Dynamics (CFD) model to analyze the trade-off between fuel utilization in the depletion layers over planar electrodes and species crossover responsible of self-discharge in the mixing layer between the two co-flowing electrolytes, considering in their study different cross-sectional geometries of MRFBs. The numerical results showed that the performance of micro RFBs is limited by diffusion, and tapered micro-channels were proposed as a possible solution.

Krishnamurthy et al. [34] developed a CFD model to investigate flow-through porous electrodes in VMRFBs and compared their results with previous experimental data [18]. Their objective was to obtain the optimal operating conditions in terms of power density and energy efficiency for a given flow rate. Simulations demonstrated that improvements on the electrodes and channel geometries can lead to enhanced performance of micro MRFBs. Lisboa and Cotta [35] developed a hybrid numerical-analytical solution applied to a flow-by configuration with porous electrodes. The crossover rate was found to increase with the thickness of the porous electrodes and when reducing the Reynolds number, and the efficacy of porous electrodes for the mitigation of mass transport limitations compared with planar electrodes was demonstrated. Lisboa and Cotta [36] extended their analysis to account for symmetrical sinusoidal wall corrugations in the solid electrodes of a MRFB. The corrugated design aimed to increase the reactive surface area, but avoiding the high pressure loss caused by the presence of a porous electrode. A significant enhancement of the limiting current density was observed compared to planar electrodes but at the same time the disturbances generated by the corrugated electrode had a marked effect on the crossover rate and consequently on the self-discharge reactions, which decreased energy efficiency.

The aim of this paper is to investigate the mixing and reaction processes that take place in the mixing layer between the two laminar co-flowing electrolytes in a micro VMRFB. Due to the absence of a separating membrane, when the electrolytes come into contact, the active species start to diffuse to the opposite stream enabling self-discharge reactions to eventually reduce the amount of charged species. This leads to a partial battery discharge whose magnitude depends both on the residence time of the electrolytes in the mixing region and on the rate of the homogeneous self-discharge reactions. To estimate the capacity lost, a simple two-dimensional model is presented and discussed. The model describes the laminar mixing and reaction process that occurs between the two co-flowing electrolytes, which is assumed not to be affected by the depletion layers generated by the heterogeneous reactions at the planar electrodes. For sufficiently large Peclet numbers, longitudinal diffusion and transverse convection can be ignored, which in the absence of migration effects leads to a classical convection-diffusion-reaction equation for which analytical and numerical results are obtained in different limiting cases. While convection and diffusion are well understood, the kinetics of the homogeneous self-discharge reactions between the various oxidation states of vanadium has not been thoroughly studied yet. For this reason, the limiting cases of infinitely slow (frozen chemistry) and infinitely fast (chemical equilibrium) reactions are investigated successively in order to provide lower and upper bounds for the crossover fluxes and self-discharge rates in micro VMRFBs. A thorough comparison of the two solutions is carried out and a parametric study involving the state of charge and the ratio between the total amount of vanadium in both electrolytes is finally presented.

2. Mathematical model

Fig. 1 represents the planar section perpendicular to the mixing region of a VMRFB in a multilayer flow-by configuration, as previously studied by Kjeang et al. [18] and Goulet at Kjeang [37,38]. Equal flow rates of both electrolytes are conducted separately from their respective deposits through the positive, $y > 0$, and negative, $y < 0$, channels of a two-dimensional cell configuration. The channel length, L, is assumed to be moderately large compared to the channel height, $2H$, leading to a slender channel geometry. Moreover, the third dimension is considered large compared to the channel height, thereby enabling the two-dimensional flow

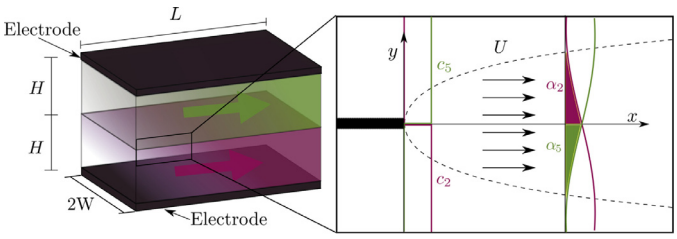

Fig. 1. Sketch of the reaction cell of a VMRFB under study. The close-up view shows the mixing region where both streams are in contact and the exchange of protons and other ions take place.

description. Corrections for finite cell depths of the order of the channel height are discussed in Section 6. Between sections $x = 0$ and L, both streams flow parallel to each other to ensure proton transfer between the electrolytes. However, this also permits the transport of vanadium ions by diffusion and migration across the separating streamline, $y = 0$, leading to the well-known crossover phenomenon. As a result of the mixing process between the different vanadium ions, homogeneous self-discharge reactions may take place, starting in the reaction cell and continuing downstream, once the two streams are separated and stored in the deposits.

Due to the small diffusivities of vanadium ions, under normal operating conditions the effect of diffusion is limited to the slender mixing layer that spreads out to both sides of the dividing streamline. In this preliminary study, the mixing layer is assumed to be much thinner than the channel height throughout the parallel flow region. Assuming also that the flow is fully developed, the mixing layer presents a uniform velocity profile $\vec{u} = U\vec{e}_x$. Following standard practice, in this paper the four oxidation states of vanadium VO_2^+, VO^{2+}, V^{3+}, and V^{2+} are also denoted as V^{V}, V^{IV}, V^{III}, and V^{II} respectively. The positive electrolyte enters the top channel containing only V^{V} and V^{IV} with concentrations $c_{5,0}$ and $c_{4,0}$, whereas the negative electrolyte enters the bottom channel containing only V^{III} and V^{II} with concentrations $c_{3,0}$ and $c_{2,0}$, respectively. As a result of self-discharge reactions, ions from one channel can not be found at the inlet of the other channel as long as V^{V} and V^{II} are present in their corresponding deposits. Vanadium ions are carried by a H_2SO_4 aqueous solution where the sulphuric acid is almost completely dissociated into protons and HSO_4^- but only partially dissociated into SO_4^{2-} as implied by the relatively small value of the dissociation constant of sulphuric acid.

Assuming that the system operates in steady state, the conservation equation for the different ions present in the electrolyte, assuming dilute-solution theory, is

$$\vec{u}\cdot\nabla c_i = n_i\nu_i F\nabla\cdot(c_i\nabla\Phi) + D_i\nabla^2 c_i + S_i,$$
$$i = \{2, 3, 4, 5, \mathrm{H}, \mathrm{HSO_4}, \mathrm{SO_4}\} \quad (1)$$

which includes convective, migration, diffusive and reaction terms, and where the numerical indexes $i = 2,\ 3,\ 4$ and 5 represent the four oxidation states of vanadium. In the above equation, c_i, D_i, n_i and ν_i denote the concentration, diffusivity, charge and mobility of species i, respectively, Φ is the electric potential, and S_i represents the corresponding chemical source term due to the homogeneous self-discharge reactions.

Following standard practice, the characteristic thickness δ_i of the mixing region can be estimated by imposing that the longitudinal convection and transverse diffusion terms are of the same order

$$U\frac{c_i}{L} \sim D_i\frac{c_i}{\delta_i^2} \quad (2)$$

leading to the well known scaling law for laminar mixing layers

$$\delta_i \sim \sqrt{\frac{D_i L}{U}}. \tag{3}$$

When ions from one channel reach the opposite electrode, a mixed potential builds up which decreases cell performance [37]. Therefore, a usual design constrain requires the thickness of the mixing layer to be small compared to the channel height [38]

$$\frac{\delta_i}{H} \sim \sqrt{\frac{D_i}{UH}\frac{L}{H}} = \sqrt{\frac{1}{\mathrm{Pe}_i}\frac{L}{H}} \ll 1 \tag{4}$$

where $\mathrm{Pe}_i = UH/D_i$ is the Peclet number of species i. Typical channel dimensions, flow velocities and mass diffusivities reported in previous studies satisfy by far this condition. As a result, diffusive terms in the streamwise direction, of order $D_i c_i/L^2$, are small compared to those in the transverse direction, of order $D_i c_i/\delta_i^2$, their ratio being of order $(\delta_i/L)^2 \lesssim (\delta_i/H)^2 \ll 1$ which can be neglected in practical applications.

The relative importance of the migration term compared to the transverse diffusion term in Eq. (1) is given by the non-dimensional electric potential drop

$$\Delta\Phi^* = \frac{\mathrm{F}\Delta\Phi}{RT} \tag{5}$$

which will be assumed to be small compared to unity, resulting in non-relevant migration transport. This simplification is clearly satisfied when the battery operates at sufficiently small current densities. Nevertheless, the influence of this term will be analysed in detail later when discussing the limitations of the current model.

In typical applications, the concentration of sulphuric acid is relatively high, and the diffusion coefficient of protons (roughly $D_\mathrm{H} = 9.3 \times 10^{-9}$ m^2/s) is an order of magnitude larger than that of vanadium ions. Therefore, the spatial distributions of HSO_4^- and SO_4^{2-} ions are not relevant and proton concentration can be assumed to be spatially uniform in the mixing layer in first approximation. As a result, the problem is reduced to determine the spatial distributions of vanadium ions using the simplified convection-diffusion-reaction equation

$$U\frac{\partial c_i}{\partial x} = D_i\frac{\partial^2 c_i}{\partial y^2} + S_i \quad \text{for} \quad i = \{2,3,4,5\} \tag{6}$$

subject to the boundary conditions

$$x = 0,\ y > 0 \quad \text{and} \quad x > 0,\ y \to \infty: \quad c_i = c_{i,0}^+ \tag{7}$$

$$x = 0,\ y < 0 \quad \text{and} \quad x > 0,\ y \to -\infty: \quad c_i = c_{i,0}^- \tag{8}$$

with

$$c_{5,0}^+ = c_{5,0}, \quad c_{4,0}^+ = c_{4,0}, \quad c_{3,0}^+ = c_{2,0}^+ = 0 \tag{9}$$

$$c_{2,0}^- = c_{2,0}, \quad c_{3,0}^- = c_{3,0}, \quad c_{4,0}^- = c_{5,0}^- = 0 \tag{10}$$

reflecting that, far from the mixing layer, the concentrations of vanadium ions are equal to their corresponding values at the channel inlets.

The chemical source terms appearing in Eq. (6) involve the reaction rates of the three overall self-discharge reactions [39]

$$\overset{\mathrm{V^V}}{\mathrm{VO_2^+}} + \overset{\mathrm{V^{III}}}{\mathrm{V^{3+}}} \xrightarrow{35} 2\overset{\mathrm{V^{IV}}}{\mathrm{VO^{2+}}} \tag{11}$$

$$\overset{\mathrm{V^{II}}}{\mathrm{V^{2+}}} + \overset{\mathrm{V^V}}{\mathrm{VO_2^+}} + 2H^+ \xrightarrow{25} \overset{\mathrm{V^{III}}}{\mathrm{V^{3+}}} + \overset{\mathrm{V^{IV}}}{\mathrm{VO^{2+}}} + \mathrm{H_2O} \tag{12}$$

$$\overset{\mathrm{V^{II}}}{\mathrm{V^{2+}}} + \overset{\mathrm{V^{IV}}}{\mathrm{VO^{2+}}} + 2H^+ \xrightarrow{24} 2\overset{\mathrm{V^{III}}}{\mathrm{V^{3+}}} + \mathrm{H_2O}. \tag{13}$$

Different sets of self-discharge reactions are commonly found in the literature [40,41], but those mechanism can be represented by the set of three reactions presented here [39]. The energy supplied to the battery during the charging process is used to oxidize $\mathrm{V^{IV}}$ to $\mathrm{V^V}$ in the positive electrode, and to reduce $\mathrm{V^{III}}$ to $\mathrm{V^{II}}$ in the negative electrode, whereas the opposite transformations occur during the discharge process. In reactions (11) and (13) ions in the charged state, $\mathrm{V^{II}}$ and $\mathrm{V^V}$, react with ions in the uncharged state from the opposite electrode to produce their corresponding uncharged ions, $\mathrm{V^{III}}$ and $\mathrm{V^{IV}}$. By contrast, in reaction (12) charged ions from both electrolytes, $\mathrm{V^V}$ and $\mathrm{V^{II}}$, react to give uncharged ions of both types. Self-discharge reactions therefore represent a loss of charged vanadium ions that must be taken into account when the efficiency of the battery is studied. The corresponding chemical source terms for the different vanadium ions are given by

$$S_5 = -\omega_{35} - \omega_{25} \tag{14}$$

$$S_4 = 2\omega_{35} + \omega_{25} - \omega_{24} \tag{15}$$

$$S_3 = -\omega_{35} + \omega_{25} + 2\omega_{24} \tag{16}$$

$$S_2 = -\omega_{25} - \omega_{24} \tag{17}$$

in terms of the reaction rates ω_{35}, ω_{25} and ω_{24} of the homogeneous self-discharge reactions (11)-(13). The reaction rates ω_{jk} may in general be expressed as an overall reaction constant times the product of the concentrations of the reactants raised to the corresponding reaction orders

$$\omega_{jk} = \kappa_{jk}(T, c_{\mathrm{H^+}}, c_{\mathrm{products}})c_j^{n_j}c_k^{n_k} \qquad jk = \{35, 25, 24\} \tag{18}$$

where the reaction constants κ_{jk} may depend not only on temperature and proton concentration, but also on the concentration of product species if reverse reactions are relevant in the detailed reaction mechanism. Although self-discharge reactions are usually assumed to be instantaneous in models of RFBs [31,32,41] with conventional architectures, i.e., including membrane separators, or simply ignored [42], precise information on the kinetics of the homogeneous self-discharge reactions in all-vanadium RFBs is not yet available in the literature.

An estimation of the importance of the reaction terms with respect to the diffusion terms in the set of Eq. (6) is given by the so-called Damköhler number

$$\mathrm{Da}_i = \frac{S_i\delta_i^2}{D_i c_i} = \frac{S_i L}{U c_i}, \tag{19}$$

where S_i, D_i and c_i represent characteristic values of the chemical production term, diffusion coefficient and concentration of species i, respectively. Note that the Damköhler number can also be viewed as the ratio of the characteristic mechanical time, $\delta_i^2/D_i \sim L/U$, over the characteristic reaction time, c_i/S_i. Here, the mechanical time is given either by the characteristic diffusion time over the mixing layer thickness, δ_i^2/D_i, or by the characteristic residence time, L/U, which are both of the same order in the mixing region.

In the absence of detailed knowledge about the overall reaction rates, $S_i \sim \omega_{jk}$, two different physically relevant limits can be identified by considering the solution that emerges for extreme values of the Damköhler number Da_i. These are limiting scenarios that may be used to delimit the real solution of this problem. In the limit $\mathrm{Da}_i \to 0$, the characteristic mechanical time is small compared to the characteristic reaction time, and the reaction term vanishes in Eq. (6), which then describe the frozen mixing between the four vanadium ions. In the slow chemistry limit, self-discharge reactions do not occur in the mixing region but later in the deposits, where the residence time is greater than in the reaction cell.

In the opposite limit of $\mathrm{Da}_i \to \infty$, the reaction time is small compared to the mechanical time. As a result, the reactants cannot

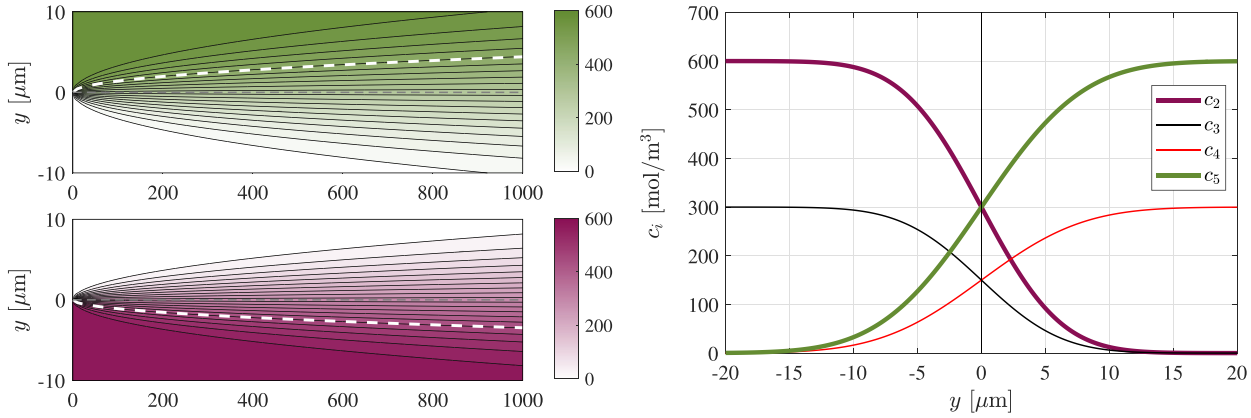

Fig. 2. Left: concentrations of V^{V} (top) and V^{II} (bottom) in the slow chemistry limit. White dashed lines mark the estimated thickness of the respective mixing regions, $\delta_i(x) = \sqrt{D_i x/U}$. Right: concentrations of the different vanadium ions at the outlet section, $x = L$, as a function of the transverse coordinate y. Inlet concentrations $c_{5,0} = c_{2,0} = 600$ mol/m^3, $c_{4,0} = c_{3,0} = 300$ mol/m^3, cell length $L = 1$ mm, cell height $H = 0.1$ mm, liquid velocity $U = 20$ mm/s, and diffusion coefficients $D_5 = D_4 = 3.9 \times 10^{-10}$ m^2/s and $D_2 = D_3 = 2.4 \times 10^{-10}$ m^2/s.

coexist in the same point of space, as they would otherwise react instantaneously. Therefore, self-discharge reactions take place at an infinitely fast rate but only in infinitesimally thin layers separating regions of chemical equilibrium. This limit is hereafter referred to as the Burke–Schumann (or fast chemistry) limit, adopting the terminology used in non-premixed combustion studies [43,44]. The solutions for the two relevant limits will be obtained, discussed and compared in the next sections, thus yielding lower and upper bounds for the losses of charged species associated with the crossover and self-discharge reactions.

3. Slow chemistry limit, $Da_i \to 0$

If the self-discharge reactions (11)–(13) are very slow they take place far downstream in the deposits rather than in the reaction cell. In the mixing region, diffusion and convection are the only relevant phenomena, and the structure of the solution is that of a laminar mixing layer whose thickness grows as $\delta_i(x) \sim \sqrt{D_i x/U}$ surrounded by two regions of uniform bulk concentrations. In this case, Eq. (6) are decoupled from each other and the solutions can be written analytically for each vanadium ion in terms of error functions in the general form

$$c_i(x,y) = \frac{c_{i,0}^{+} + c_{i,0}^{-}}{2} + \frac{c_{i,0}^{+} - c_{i,0}^{-}}{2}\,\mathrm{erf}\left(\frac{y}{2}\sqrt{\frac{U}{D_i x}}\right) = c_{i,0}^{-} + \frac{\Delta c_i}{2}\left[\mathrm{erf}\left(\frac{y}{2}\sqrt{\frac{U}{D_i x}}\right) + 1\right] \tag{20}$$

where $\Delta c_i = c_{i,0}^{+} - c_{i,0}^{-}$ is the difference between the inlet concentrations of species i in the positive and negative channels. Note that Δc_i can be either positive or negative depending on the ion under consideration. A sample solution with symmetric inlet concentrations is presented in Fig. 2.

The molar flux of species i that crosses the dividing streamline per unit depth, being transferred to the opposite channel by diffusion, can be evaluated by computing the convective flux at the outlet section

$$\alpha_i = \pm \int_0^{\pm\infty} U c_i(y,L)\,\mathrm{d}y = c_{i,0}\sqrt{\frac{D_i U L}{\pi}} \tag{21}$$

where the - sign holds for the ions of the positive channel, $i = \{4,5\}$, and + for those of the negative channel, $i = \{2,3\}$. In the slow chemistry limit, $Da_i \to 0$, the self-discharge reactions do not take place in the mixing layer. As previously discussed, even in the slow chemistry limit the ions that cross to the opposite channel have enough time to react with the charged vanadium ions of that channel once they reach the deposits, eventually reducing the amount of energy stored in the system.

To quantify the reduction of stored energy, it is important to take into account all possible reactions between the ions present in one channel and the ions that diffuse across the mixing layer from the opposite channel. These reactions result in the following expressions for the moles of vanadium ions being lost (-) or gained (+) in their respective channels per unit time and unit depth as a result of the combined effect of mass diffusion in the reaction cell and self-discharge reactions

$$\Delta\varphi_{5,s} = -\alpha_5 - \alpha_3 - 2\alpha_2, \tag{22}$$

$$\Delta\varphi_{4,s} = -\alpha_4 + 2\alpha_3 + 3\alpha_2 \tag{23}$$

$$\Delta\varphi_{3,s} = -\alpha_3 + 2\alpha_4 + 3\alpha_5 \tag{24}$$

$$\Delta\varphi_{2,s} = -\alpha_2 - \alpha_4 - 2\alpha_5 \tag{25}$$

where subindex s indicates results obtained in the slow chemistry limit. The first terms on the right-hand-sides represent the fluxes lost by diffusion to the opposite channel, while the other terms reflect the effect of the self-discharge reactions, whose overall stoichiometry dictates the signs and numerical factors. For instance, Eq. (22) shows that, besides being lost by diffusion to the negative channel, V^{V} is also lost by reaction (11) in a one-to-one molar ratio with the V^{III} that diffuses from the negative channel, and also reacts in a two-to-one molar ratio with the V^{II} that diffuses from the negative channel according to the overall reaction obtained by adding reactions (11) and (12). As a result of the self-discharge reactions, two moles of V^{IV} are produced in the positive side per unit mole of V^{III} consumed, and three moles are produced per unit mole of V^{II} consumed, resulting in the positive terms appearing on the right-hand-side of Eq. (23). The same type of arguments lead to Eq. (24) and (25).

Adding Eq. (22)–(25) yields the total flux of vanadium ions lost (-) or gained (+) in the positive and negative channels per unit time and unit depth

$$\Delta\varphi_{+,s} = \Delta\varphi_{5,s} + \Delta\varphi_{4,s} = -\alpha_5 - \alpha_4 + \alpha_3 + \alpha_2 \tag{26}$$

$$\Delta\varphi_{-,s} = \Delta\varphi_{2,s} + \Delta\varphi_{3,s} = -\alpha_2 - \alpha_3 + \alpha_4 + \alpha_5 \tag{27}$$

the first two terms on the right-hand-sides representing losses by diffusion to the opposite channel and the other two gains by diffusion from the opposite channel. Adding the two equations leads to

the expected result that the total amount of vanadium ions in the system must remain constant, $\Delta\varphi_{+,s} + \Delta\varphi_{-,s} = 0$.

4. Fast chemistry limit, $Da_i \to \infty$

In the opposite limit of $Da_i \to \infty$, self-discharge reactions (11) and (13) take place, at an infinitely fast rate, only in infinitesimally thin layers, Σ_{35} and Σ_{24}, respectively. On both sides of the reaction fronts there is chemical equilibrium

$$\omega_{jk} = 0 \quad \rightarrow \quad c_j^{n_j} c_k^{n_k} = 0 \qquad jk = \{24, 35\} \tag{28}$$

hence the reactants cannot coexist, with a region Ω_j in which $c_k = 0$ and a region Ω_k in which $c_j = 0$. The reaction-rate terms in Eq. (6) then become Dirac delta distributions located at Σ_{jk}. These Dirac delta distributions, sinks for the reactant and sources for the products, are necessarily balanced in Eq. (6) by diffusion terms, mainly by the changes in the diffusion flux normal to Σ_{jk}. Therefore, they produce jumps at the reaction sheet of these fluxes, leading to the condition that the different ions must reach the reaction sheet in stoichiometric proportions. It is important to note that since V^V is completely consumed by reaction (11) at Σ_{35} and V^{II} by reaction (13) at Σ_{24}, reaction (12) will not be able to occur anywhere in the flowfield, as the two reactants involved, V^V and V^{II}, are consumed separately before they can even come into contact.

In the fast chemistry limit, the structure of the solution is anticipated to include two outer mixing regions Ω_5 and Ω_2, where charged and discharged ions of the positive and negative channel coexist, separated by a central mixing region $\Omega_3 \cap \Omega_4$ which only contains ions in the discharged state. The three mixing regions are separated by two infinitely thin reaction sheets, namely a reaction sheet in the positive side, Σ_{35}, located at $y = d^+(x)$, where the charged vanadium ion V^V is instantly consumed through reaction (11) to give V^{IV}, and another reaction sheet in the negative side, Σ_{24}, located at $y = d^-(x)$, where the charged vanadium ion V^{II} is instantly consumed through reaction (13) to give V^{III}. The two reaction sheets shift away from the dividing streamline as the mixing layer widens downstream, resulting in a thickening of the central region. Each reaction sheet consumes the charged vanadium ions supplied by its channel and produces the corresponding discharged ions that either react with the charged ions of the opposite channel at the opposite reaction sheet or diffuse back towards the bulk flow of its own channel.

The solution described above is determined by the conservation equations governing the transport of vanadium ions in the fast chemistry limit

$$U\frac{\partial c_5}{\partial x} = D_5\frac{\partial^2 c_5}{\partial y^2} - \quad \omega_{35} \tag{29}$$

$$U\frac{\partial c_4}{\partial x} = D_4\frac{\partial^2 c_4}{\partial y^2} + 2\omega_{35} - \quad \omega_{24} \tag{30}$$

$$U\frac{\partial c_3}{\partial x} = D_3\frac{\partial^2 c_3}{\partial y^2} - \quad \omega_{35} + 2\omega_{24} \tag{31}$$

$$U\frac{\partial c_2}{\partial x} = D_2\frac{\partial^2 c_2}{\partial y^2} - \quad \omega_{24} \tag{32}$$

where, as previously discussed, the reaction term ω_{25} does not appear here as it is identically zero everywhere, while the reaction terms ω_{35} and ω_{24} become Dirac delta distributions in the reaction sheets Σ_{35} and Σ_{24}, respectively. As first shown by Burke & Schumann [43], in the case of equal diffusivities of the reactants, $D_i = D$, the difficulties associated with the singular character of the solution can be circumvented by eliminating the chemical terms by linear combinations of the conservation equations, which reduces the problem to that of integrating a series of convection-diffusion equations for a conveniently defined set of passive scalars unaffected by the chemical reactions [45,46]. In the case of unequal diffusivities described by Eq. (29)–(32), the analysis can be generalized following the ideas set forth by Liñán [47,48].

4.1. Formulation in terms of passive scalars

For simplicity in the presentation, it will be assumed that the vanadium ions present in each channel have the same diffusivities in the charged and discharged states, i.e., $D_5 = D_4$ and $D_2 = D_3$, an approximation well supported by experimental evidence [49]. In this case, two chemistry-free conservation equations can be obtained by linear combination of Eq. (29)–(32)

$$U\frac{\partial z_1}{\partial x} = D_5\frac{\partial^2 \tilde{z}_1}{\partial y^2}, \tag{33}$$

$$U\frac{\partial z_2}{\partial x} = D_2\frac{\partial^2 \tilde{z}_2}{\partial y^2}, \tag{34}$$

written in terms of the four passive scalars

$$z_1 = c_5 - (c_3 + 2c_2), \quad \tilde{z}_1 = c_5 - \gamma(c_3 + 2c_2), \tag{35}$$

$$z_2 = c_2 - (c_4 + 2c_5), \quad \tilde{z}_2 = c_2 - \frac{1}{\gamma}(c_4 + 2c_5), \tag{36}$$

where the tilded variables are expressed in terms of the negative to positive channel diffusivity ratio, $\gamma = D_2/D_5$. This ratio is smaller than unity ($\gamma = 0.6154$) contrary to what would be expected of the size of the different ions. That counter-intuitive result is justified by the actual size of the most stable forms of those ions that are, by increasing oxidation number, $[V(H_2O)_6]^{2+}$, $[V(H_2O)_6]^{3+}$, $[VO(H_2O)_5]^{2+}$, and $[VO_2(H_2O)_3]^{+}$ as stated in [39].

Eqs. (33) and (34) must be complemented with the chemical equilibrium conditions given in (28) of noncoexistence of the reactants, and the definitions given in Eqs. (35) and (36), to give the following expressions for the concentrations of vanadium ions in terms of z_1 and z_2 (or $\tilde{z}_1$ and $\tilde{z}_2$) in the different fluid domains

$$\Omega_5: \quad c_2 = c_3 = 0, \quad c_5 = z_1 = \tilde{z}_1, \quad c_4 = -z_2 - 2z_1 = -\gamma\tilde{z}_2 - 2\tilde{z}_1, \tag{37}$$

$$\Omega_3 \cap \Omega_4: \quad c_5 = c_2 = 0, \quad c_3 = -z_1 = -\frac{\tilde{z}_1}{\gamma}, \quad c_4 = -z_2 = -\gamma\tilde{z}_2, \tag{38}$$

$$\Omega_2: \quad c_5 = c_4 = 0, \quad c_2 = z_2 = \tilde{z}_2, \quad c_3 = -z_1 - 2z_2 = -\frac{\tilde{z}_1}{\gamma} - 2\tilde{z}_2, \tag{39}$$

It is worth noting that the reaction sheets Σ_{35} and Σ_{24} are located at the interfaces between the central mixing region ($\Omega_3 \cap \Omega_4$) and the positive (Ω_5) and negative (Ω_2) channel domains, respectively, where the concentrations of the corresponding reactants are simultaneously zero, $c_3 = c_5 = 0$ at Σ_{35} and $c_2 = c_4 = 0$ at Σ_{24}, leading to values of the passive scalars $z_1 = \tilde{z}_1 = 0$ and $z_2 = \tilde{z}_2 = 0$, respectively. The expressions given in Eqs. (37)-(39) for the concentration of ions in terms of the coupling functions provide also the following piecewise linear relations between the passive scalars z_i and $\tilde{z}_i$

$$\Omega_5: \quad \tilde{z}_1 = z_1, \quad \tilde{z}_2 = \frac{z_2}{\gamma}, \tag{40}$$

$$\Omega_3 \cap \Omega_4: \quad \tilde{z}_1 = \gamma z_1, \quad \tilde{z}_2 = \frac{z_2}{\gamma}, \tag{41}$$

$$\Omega_2: \quad \tilde{z}_1 = \gamma z_1, \quad \tilde{z}_2 = z_2. \tag{42}$$

Expressions (37)-(42), accompanied by Eqs. (33) and (34), replace Eq. (6) in the integration of the problem, thereby removing the singularity associated with the reaction term.

Using the piecewise linear relations defined above, Eq. (33) and (34) can be rewritten in terms of z_1 and z_2 as follows

$$\Omega_5: \quad U\frac{\partial z_1}{\partial x} = D_5\frac{\partial^2 z_1}{\partial y^2}, \quad U\frac{\partial z_2}{\partial x} = D_5\frac{\partial^2 z_2}{\partial y^2}, \tag{43}$$

$$\Omega_3 \cap \Omega_4: \quad U\frac{\partial z_1}{\partial x} = D_2\frac{\partial^2 z_1}{\partial y^2}, \quad U\frac{\partial z_2}{\partial x} = D_5\frac{\partial^2 z_2}{\partial y^2}, \tag{44}$$

$$\Omega_2: \quad U\frac{\partial z_1}{\partial x} = D_2\frac{\partial^2 z_1}{\partial y^2}, \quad U\frac{\partial z_2}{\partial x} = D_2\frac{\partial^2 z_2}{\partial y^2}, \tag{45}$$

where the diffusion coefficient for z_1 changes across Σ_{35}, located at $y = d^+(x)$, whereas that for z_2 changes across Σ_{24}, located at $y = d^-(x)$. The boundary conditions and the conditions of continuity of ion fluxes at the interfaces can be expressed in terms of the passive scalars z_1 and z_2 as

$$x = 0,\ y > 0 \qquad \text{and}$$
$$x > 0,\ y \to \infty: \quad z_1 = z_1^+, \quad z_2 = z_2^+ \tag{46}$$

$$x > 0,\ y = d^+(x): \quad z_1 = 0, \quad \left.\frac{\partial z_1}{\partial y}\right|_+ = \gamma \left.\frac{\partial z_1}{\partial y}\right|_- \tag{47}$$

$$x > 0,\ y = d^-(x): \quad z_2 = 0, \quad \left.\frac{\partial z_2}{\partial y}\right|_+ = \gamma \left.\frac{\partial z_2}{\partial y}\right|_- \tag{48}$$

$$x = 0,\ y < 0 \qquad \text{and}$$
$$x > 0,\ y \to -\infty \qquad : \quad z_1 = z_1^-, \quad z_2 = z_2^- \tag{49}$$

where

$$z_1^+ = c_{5,0}, \quad z_2^+ = -(c_{4,0} + 2c_{5,0}), \tag{50}$$

$$z_2^- = c_{2,0}, \quad z_1^- = -(c_{3,0} + 2c_{2,0}), \tag{51}$$

represent the values of the passive scalars at the channel inlets and far away from the mixing layer, and the subscripts in the derivatives of z_1 and z_2 denote the side of the reaction sheet where they are evaluated.

4.2. Solution in terms of passive scalars

The solution to the problem stated above can be conveniently written in terms of piecewise error functions

$$z_1(x,y) = \begin{cases} A_1 + \frac{z_1^+ - A_1}{2}\left[\mathrm{erf}\left(\frac{y}{2}\sqrt{\frac{U}{D_5 x}}\right) + 1\right] & \text{for} \quad y > d^+(x) \\ z_1^- + \frac{B_1 - z_1^-}{2}\left[\mathrm{erf}\left(\frac{y}{2}\sqrt{\frac{U}{D_2 x}}\right) + 1\right] & \text{for} \quad y < d^+(x) \end{cases} \tag{52}$$

$$z_2(x,y) = \begin{cases} A_2 + \frac{z_2^+ - A_2}{2}\left[\mathrm{erf}\left(\frac{y}{2}\sqrt{\frac{U}{D_5 x}}\right) + 1\right] & \text{for} \quad y > d^-(x) \\ z_2^- + \frac{B_2 - z_2^-}{2}\left[\mathrm{erf}\left(\frac{y}{2}\sqrt{\frac{U}{D_2 x}}\right) + 1\right] & \text{for} \quad y < d^-(x) \end{cases} \tag{53}$$

where the integration constants, A_1, A_2, B_1 and B_2, and the position of the reaction sheets, $d^-(x)$ and $d^-(x)$, must be determined so as to satisfy the compatibility conditions (47) and (48) at the reaction sheets. This leads to the following set of six non-linear equations

$$0 = A_1 + \frac{z_1^+ - A_1}{2}\left[\mathrm{erf}\left(C^+\right) + 1\right], \tag{54}$$

$$0 = A_2 + \frac{z_2^+ - A_2}{2}\left[\mathrm{erf}\left(C^-\right) + 1\right], \tag{55}$$

$$0 = z_1^- + \frac{B_1 - z_1^-}{2}\left[\mathrm{erf}\left(C^+/\sqrt{\gamma}\right) + 1\right], \tag{56}$$

$$0 = z_2^- + \frac{B_2 - z_2^-}{2}\left[\mathrm{erf}\left(C^-/\sqrt{\gamma}\right) + 1\right], \tag{57}$$

$$0 = A_1 - z_1^+ + \sqrt{\gamma}(B_1 - z_1^-)\exp\left[(C^+)^2(1 - 1/\gamma)\right], \tag{58}$$

$$0 = A_2 - z_2^+ + \sqrt{\gamma}(B_2 - z_2^-)\exp\left[(C^-)^2(1 - 1/\gamma)\right], \tag{59}$$

for the six constants A_1, A_2, B_1, B_2, C^+ and C^-, the last two determining the position of the reaction sheets Σ_{35} and Σ_{24} according to

$$d^\pm(x) = 2C^\pm\sqrt{\frac{D_5 x}{U}}. \tag{60}$$

The solution to Eqs. (54)-(59), described in Appendix A, gives the distributions of vanadium ions through Eqs. (37)-(39), with z_1 and z_2 given by (52) and (53). With these distributions, one can write expressions for the moles of vanadium ions lost (-) or gained (+) per unit time and unit depth by the combined effect of diffusion and self-discharge reactions. Thus, the losses of V^V are

$$\Delta\varphi_{5,f} = \underbrace{\int_{d^+(L)}^{\infty} Uc_5(L,y)\,\mathrm{d}y - \int_0^{d^+(L)} Uc_3(L,y)\,\mathrm{d}y}_{I_1} - \underbrace{\int_0^{\infty} Uc_{5,0}\,\mathrm{d}y}_{I_2} = -\int_0^{\infty} U\left[z_1^+ - z_1(L,y)\right]\mathrm{d}y \tag{61}$$

representing the difference between the molar flux of V^V that reaches the deposit after complete reaction with the V^{III} that crosses from the negative channel (I_1), and the molar flux of V^V that enters the reaction cell (I_2). Similarly, for V^{IV} one may write

$$\Delta\varphi_{4,f} = \underbrace{\int_{d^+(L)}^{\infty} Uc_4(L,y)\,\mathrm{d}y + \int_0^{d^+(L)} Uc_4(L,y)\mathrm{d}y + 2\int_0^{d^+(L)} Uc_3(L,y)\mathrm{d}y}_{I_3} - \underbrace{\int_0^{\infty} Uc_{4,0}\,\mathrm{d}y}_{I_4} = \int_0^{\infty} U\left[z_2^+ + 2z_1^+ - \left[z_2(L,y) + 2z_1(L,y)\right]\right]\mathrm{d}y \tag{62}$$

representing the difference between the molar flux of V^{IV} that reaches the deposit (I_3), including the V^{IV} produced by reaction (11) between V^V and V^{III}, and the molar flux of V^{IV} that enters the reaction cell (I_4). In the above equations, use has been made of relations (37)-(39) and (50)-(51) to express the losses in terms of integrals of the passive scalars z_1 and z_2 and their values at the inlet of the positive channel z_1^+ and z_2^+. Similar expressions can be derived for the ions of the negative channel, V^{II} and V^{III}, namely

$$\Delta\varphi_{2,f} = -\int_{-\infty}^{0} U\left[z_2^- - z_2(L,y)\right]\mathrm{d}y \tag{63}$$

$$\Delta\varphi_{3,f} = \int_{-\infty}^{0} U\left[z_1^- + 2z_2^- - \left[z_1(L,y) + 2z_2(L,y)\right]\right]\mathrm{d}y \tag{64}$$

leading to the total fluxes of ions lost (-) or gained (+) by the positive and negative channels

$$\Delta\varphi_{+,f} = \Delta\varphi_{5,f} + \Delta\varphi_{4,f} = \int_0^{\infty} U\left[z_2^+ + z_1^+ - \left[z_2(L,y) + z_1(L,y)\right]\right]\mathrm{d}y \tag{65}$$

$$\Delta\varphi_{-,f} = \Delta\varphi_{2,f} + \Delta\varphi_{3,f} = \int_{-\infty}^{0} U\left[z_1^- + z_2^- - \left[z_1(L,y) + z_2(L,y)\right]\right]\mathrm{d}y \tag{66}$$

with overall vanadium conservation implying that $\Delta\varphi_{+,f} + \Delta\varphi_{-,f} = 0$.

4.3. Discussion of illustrative results

Fig. 3 shows, in the left panel, the concentrations of V^V and V^{II} in the mixing layer, and in the right panel, the outlet profiles of the ion concentrations, c_i, and passive scalars, z_i, for a sample fast chemistry solution with the same set of symmetric boundary conditions used in Fig. 2. The left plot represents the distribution of vanadium ions in their charged state, V^V and V^{II}, including the position of the reaction sheets given by Eq. (60) separating the three

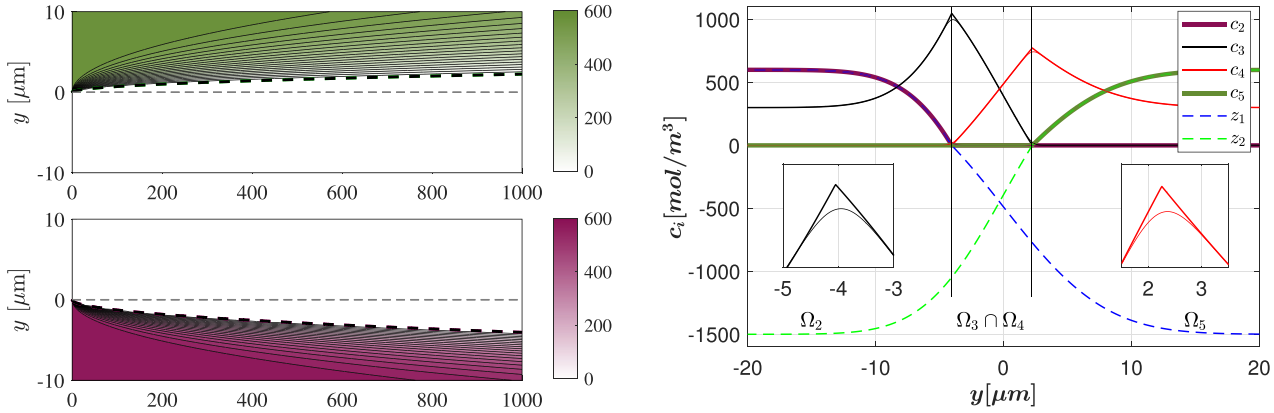

Fig. 3. Left: concentrations of V^{V} (top) and V^{II} (bottom) in the fast chemistry limit, $Da_i \to \infty$. Dashed lines mark the location of the reaction sheets Σ_{35} and Σ_{24} given by equation (60). Right: concentrations of the different vanadium ions and passive scalars z_i (dashed lines) at the outlet section ($x = L$) as a function of the transverse coordinate y. The insets show detailed views of the peaks of V^{III} (left) and V^{IV} (right) appearing in the reaction fronts. The numerical solution for $Da_i \simeq 3 \times 10^4$ is shown in thin lines. Same conditions as in Fig. 2.

regions of the solution. The right panel shows the concentrations of all vanadium ions and the profiles of the two passive scalars z_1 and z_2 at the channel outlet, $x = L$. Note that the negative values of the passive scalars z_i shown in Fig. 3 lead to positive ion concentrations c_i as the former appear with a negative sign in Eqs. (37)-(39) in the regions with $z_i < 0$.

Although the concentration profiles are continuous in the fast chemistry limit, their gradients exhibit jumps at the reaction sheets, corresponding to the localized chemical sources. This results, for instance, in peaked distributions of discharged ions, with the peak of V^{III}, $c_{3,\max} = -z_1(d^-(L))$, being larger than that of V^{IV}, $c_{4,\max} = -z_2(d^+(L))$, as a result of the higher diffusivity of the latter, which requires less gradients to evacuate the ions generated at the reaction sheet. It is interesting to note that the passive scalars z_1 and z_2 are also continuous, but their gradients exhibit jumps at the reaction sheets Σ_{35} and Σ_{24}, respectively. By contrast, gradients of the passive scalars $\tilde{z}_1$ and $\tilde{z}_2$ are continuous everywhere, which makes them better suited for a numerical solution of the problem in the fast chemistry limit if unsteady flows, or more complex geometries, not amenable to analytical treatment, were investigated.

As a final remark, it is interesting to note that in both limiting cases, $Da_i \to 0$ and $Da_i \to \infty$, the problem reduces to one of mixing, described in the last case in terms of passive scalars unaffected by chemical reactions. As a result, despite the different structure of the solutions, the limits of slow and fast self-discharge reactions share a similar dependence on certain parameters. In particular, like in the slow chemistry limit, see, e.g., Eq. (21), the fluxes of vanadium ions lost by diffusion and self-discharge reactions in the fast chemistry limit, $\Delta\varphi_{i,f}$, also scale with $c_{i,0}(D_i UL/\pi)^{1/2}$, as can be inferred from order of magnitude estimates in Eqs. (61)-(66).

4.4. Validation against numerical simulations

The analytic solution that emerges in the fast chemistry limit $Da_i \to \infty$ has been validated against the numerical solution of the problem stated by Eqs. (6)-(18). The numerical solution has been obtained by integration of the one-dimensional time dependent diffusion-reaction equation resulting from the substitution of the longitudinal coordinate x by a false time variable $t = x/U$ in Eq. (6) for each vanadium ion. The inlet concentrations of vanadium ions are specified as initial conditions at $t = 0$ according to (7)-(10), and are allowed to evolve in time until the final time $t_L = L/U$ is reached, thereby yielding the solution at the outlet section. Far from the mixing region, the initial concentrations are also supplied as boundary condition according to (7)-(10). Several numerical tests have been performed to make sure that the extent of the computational domain in the channel cross-section direction did not influence the final solution. The cross section is discretized using a nonuniform number of elements with higher density within the reaction fronts. The higher element density was chosen high enough to resolve in detail the strong changes in concentration gradients that occur in the reaction layers and, therefore, was dependent on the value of Da_i.

For simplicity, first order kinetics in all vanadium ions has been assumed for reactions (11)-(13), taking $n_j = n_k = 1$ in (18), no reverse reactions are included and the concentration of protons is considered spatially uniform throughout the mixing region and can therefore be incorporated into the reaction constants. The effective reaction constants are all assigned the arbitrarily large value $\kappa_{jk} = 10^3$ mol/(m$^3 \cdot$ s) for validation purposes, which results in a fairly large value of the Damköhler number, $Da_i = S_i L/(Uc_i) = \kappa_{ij} c_j L/U \simeq 3 \times 10^4$. The insets in Fig. 3 show the smoothed solution within the reaction zones in the negative and positive channels as obtained from the numerical solution of the problem obtained with COMSOL Multiphysics [50], against the analytical solution of the fast chemistry limit, $Da_i \to \infty$, given above. The large but finite reaction rates used in the numerical solution translate into smoothed ion distributions, contrasting with the peaked distributions obtained for infinitely fast chemistry also shown in the figure for reference purposes. It is well known that in the limit $Da_i \gg 1$ the reactants only coexist in thin reaction layers of thickness $\delta_R \sim Da_i^{-1/3}\delta_i$, with small concentrations of order $c_{i,R} \sim Da_i^{-1/3} c_i$ [51,52]. For the conditions shown in the figure, the thickness of the reaction zones (~ 1 μm) is roughly 3 % of the thickness of the mixing layer (~ 30 μm), what is compatible with these estimations for the value of Da_i given above. As can be seen, the numerical and analytical solutions are undistinguishable outside of the smoothed reaction layers, which serves as validation of the theoretical results presented in this section.

5. Comparison of the slow and fast chemistry limits

Dimensional analysis shows that the amount of vanadium ions lost by diffusion and self-discharge reactions can be expressed in dimensionless form as

$$\frac{\Delta\varphi_i}{(c_{5,0}+c_{4,0})UL} = f_i\left(\mathrm{SoC}_{45}, \mathrm{SoC}_{23}, \mathrm{CR}, Da_i, \frac{UL}{D_5}, \gamma, \frac{H}{L}\right) \tag{67}$$

where

$$\mathrm{SoC}_{45} = \frac{c_{5,0}}{c_{5,0}+c_{4,0}}, \quad \mathrm{SoC}_{23} = \frac{c_{2,0}}{c_{2,0}+c_{3,0}} \quad \text{and} \quad \mathrm{CR} = \frac{c_{2,0}+c_{3,0}}{c_{5,0}+c_{4,0}} \tag{68}$$

are the states of charge (SoC) of the positive and negative electrolytes (which may in general be different if the battery is chemically unbalanced) and the negative to positive-channel total vanadium concentration ratio (CR), respectively. The above dependence can be simplified in the limit $H/L \gg (UL/D_5)^{-1/2}$, when $H \gg (D_5 L/U)^{1/2} = \delta_5 \sim \delta_2$ ceases to be a relevant parameter, and by fixing the mass diffusivity ratio $\gamma = D_2/D_5 = 0.6154$ [49]. Finally, since the dominant mechanism for ion crossover is mass diffusion, regardless of the self-discharge reactions rate, and the flow is assumed laminar and steady, the dependence of the vanadium losses can be expressed in the simplified form

$$\Delta\tilde{\varphi}_i = \frac{\Delta\varphi_i}{(c_{5,0}+c_{4,0})(D_5 UL/\pi)^{1/2}} = \tilde{f}_i(\mathrm{SoC}_{45}, \mathrm{SoC}_{23}, \mathrm{CR}; \mathrm{Da}_i) \tag{69}$$

which exhibits a linear dependence of $\Delta\varphi_i$ with $(D_i UL/\pi)^{1/2}$ in agreement with the results of the slow chemistry limit given in Eqs. (21)-(22). This section presents and compares the fluxes of the different vanadium ions in the slow and fast chemistry limits, $\Delta\varphi_{i,s}$ and $\Delta\varphi_{i,f}$, which correspond to $\mathrm{Da}_i \to 0$ and ∞ in Eq. (69), respectively. The quantitative differences between the two limits will be discussed in terms of the remaining dimensionless parameters, i.e., SoC_{45}, SoC_{23} and CR.

In the limit of slow self-discharge reactions, the losses given analytically by Eqs. (22)-(27) can be rewritten in dimensionless form (69) as follows

$$\Delta\tilde{\varphi}_{5,s} = -[\mathrm{SoC}_{45} + \sqrt{\gamma}\ \mathrm{CR}(1+\mathrm{SoC}_{23})], \tag{70}$$

$$\Delta\tilde{\varphi}_{4,s} = \mathrm{SoC}_{45} - 1 + \sqrt{\gamma}\ \mathrm{CR}(2+\mathrm{SoC}_{23}), \tag{71}$$

$$\Delta\tilde{\varphi}_{3,s} = \mathrm{SoC}_{45} + 2 + \sqrt{\gamma}\ \mathrm{CR}(\mathrm{SoC}_{23} - 1), \tag{72}$$

$$\Delta\tilde{\varphi}_{2,s} = -[\mathrm{SoC}_{45} + 1 + \sqrt{\gamma}\ \mathrm{CR}\ \mathrm{SoC}_{23}], \tag{73}$$

while the total flux of vanadium ions lost from the positive and negative channels is given by

$$\Delta\tilde{\varphi}_{+,s} = \Delta\tilde{\varphi}_{5,s} + \Delta\tilde{\varphi}_{4,s} = \sqrt{\gamma}\ \mathrm{CR} - 1 \tag{74}$$

$$\Delta\tilde{\varphi}_{-,s} = \Delta\tilde{\varphi}_{2,s} + \Delta\tilde{\varphi}_{3,s} = -\Delta\varphi_{+,s}. \tag{75}$$

The above expressions for $\Delta\tilde{\varphi}_+$ and $\Delta\tilde{\varphi}_-$ show that the total amount of vanadium lost or gained by the electrolytes does not depend on the states of charge, but only on the concentration and diffusivity ratios, CR and γ. As the two vanadium ions of each channel are assumed to share the same diffusion coefficient, losses by diffusion do not depend on the actual proportion of ions in the charged and discharged states, but only on the total concentration of vanadium ions. Eq. (74) and (75) show that the total vanadium flux from both channels is zero for a particular value of the concentration ratio, $\mathrm{CR} = 1/\sqrt{\gamma} = \sqrt{D_5/D_2} = 1.275$, for which the concentration of vanadium ions in the negative channel is 27.5% higher than in the positive channel. In this case, the diffusion fluxes from the negative to the positive channel induced by the higher gradients of V^{II} and V^{III} with lower diffusivity are exactly compensated by the fluxes in the opposite direction induced by the lower gradients of V^{IV} and V^{V} with higher diffusivity. For $\mathrm{CR} > 1.275$ there is a net flux of total vanadium ions from the negative ($\Delta\tilde{\varphi}_{-,s} < 0$) to the positive ($\Delta\tilde{\varphi}_{+,s} > 0$) side, while the opposite occurs for $\mathrm{CR} < 1.275$.

Closed form analytical expressions for the losses in the fast chemistry limit similar to those given above for the slow chemistry limit do not exist. In the fast chemistry limit, the determination of the concentration profiles requires the numerical solution of the non-linear system of Eqs. (54)-(59) for the constants A_1, A_2, B_1, B_2, C^+ and C^-, while the evaluation of the losses $\Delta\varphi_{i,f}$ requires the numerical integration of the quadratures of z_1 and z_2 given in Eqs. (61)-(66). Thus, the results presented below for the fast chemistry limit where all obtained numerically following this procedure.

This work aims to investigate the effect of the rate of the homogeneous self-discharge reactions on the losses of charged vanadium ions, and in the accompanying variation of the total concentration of vanadium ions in the channels. Upper and lower bounds are provided below by comparing these losses in the limiting cases of slow and fast chemistry. Three parametric studies covering all possible scenarios are presented in the following subsections. First, the simplest case of symmetric inlet concentrations with $\mathrm{CR} = 1$ and equal states of charge, $\mathrm{SoC}_{45} = \mathrm{SoC}_{23}$, is adressed. The second scenario analyzes a balanced configuration with same total concentration of vanadium ions in both channels, $\mathrm{CR} = 1$, but unequal states of charge $\mathrm{SoC}_{23} \neq \mathrm{SoC}_{45}$. Finally, the third study discusses the maximum differences between the fast and slow chemistry solutions in the $(\mathrm{SoC}_{23}, \mathrm{SoC}_{45})$-plane for different values of the concentration ratio CR. Unless otherwise stated, other parameters are kept constant through the parametric study with the values presented in Table 1.

Table 1
Numerical values of the physical parameters used in the simulations of the parametric studies.

Parameter	Value	Units
L	1×10^{-3}	m
H	1×10^{-4}	m
U	2×10^{-2}	m/s
$c_{5,0} + c_{4,0}$	200	mol/m^3
D_5	3.9×10^{-10}	m^2/s
γ	0.6154	1

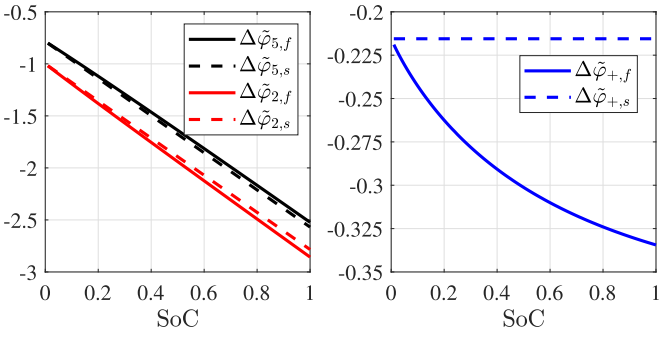

Fig. 4. (Left) Dimensionless flux of charged vanadium ions lost by diffusion and self-discharge reactions as a function of SoC in the slow and fast chemistry limits and CR = 1. (Right) Dimensionless flux of total vanadium ions lost from the positive channel. The operating parameters used for the calculations are shown in Table 1.

5.1. Case of symmetric concentrations

Vanadium RFBs are said to operate with symmetric concentrations when the total concentration of vanadium ions and the states of charge are equal in both electrolytes, $\mathrm{CR} = 1$ and $\mathrm{SoC}_{45} = \mathrm{SoC}_{23} = \mathrm{SoC}$. In such a perfectly balanced situation, the concentrations of charged and discharged vanadium ions is the same at the inlet of both channels. The plots of Fig. 4 show the fluxes of V^{V} and V^{II} lost by diffusion and self-discharge reactions, and the total flux of vanadium ions lost from the positive channel as a function of SoC in the limits of slow and fast chemistry. Note that both are negative values, implying ion losses. The inlet concentrations of charged vanadium ions increase with SoC, leading to steeper gra-

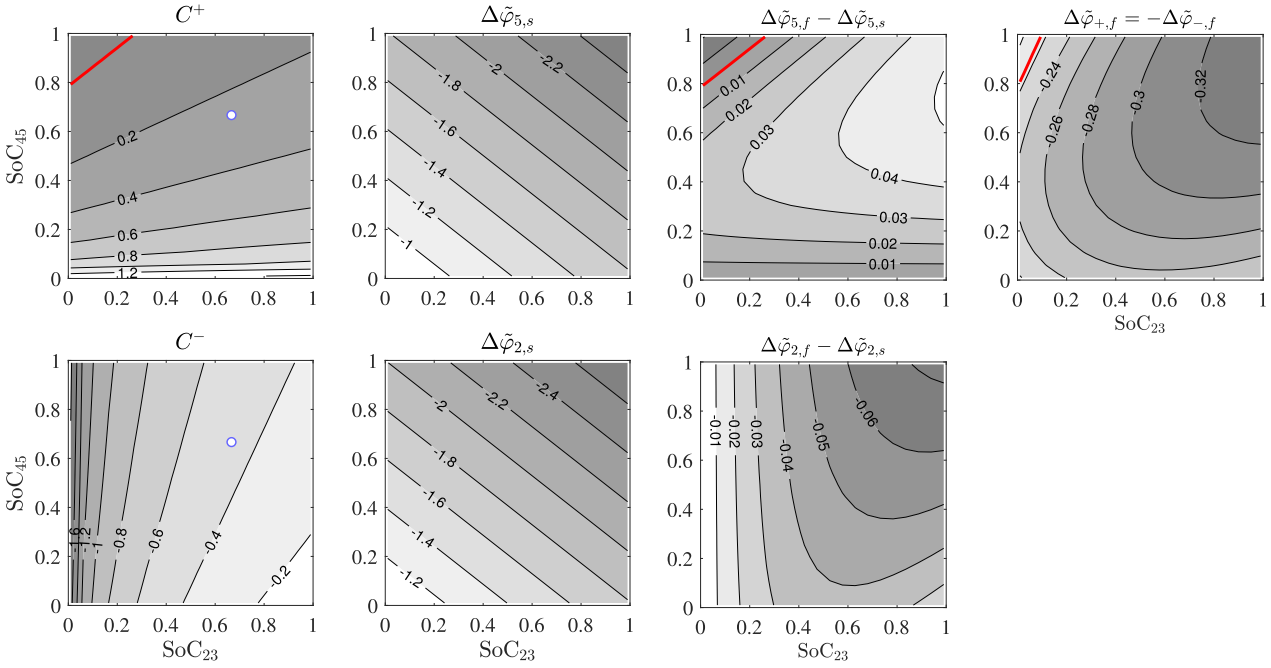

Fig. 5. Contour plots in the (SoC_{23}, SoC_{45})-plane of the constants C^+ and C^- defining the position of the reaction sheets Σ_{35} and Σ_{24} through equation (60), the dimensionless crossover flux of charged ions V^V and V^{II} in the slow chemistry limit, $\Delta\tilde{\varphi}_{i,s}$, the incremental losses between the fast and slow chemistry limits, $\Delta\tilde{\varphi}_{i,f} - \Delta\tilde{\varphi}_{i,s}$, and the total dimensionless flux of vanadium ions V^V and V^{IV} from the positive to the negative channel in the fast chemistry limit, $\Delta\tilde{\varphi}_{+,f}$, for the case of equal total vanadium concentrations, CR = 1. The hollow dots in the contour plots of C^+ and C^- indicate the conditions of Fig. 3, where $C^+ = 0.255$ and $C^- = -0.459$, as indicated by the illustrative numerical example presented in Fig. 8 (see Appendix A). The operating parameters used for the calculations are presented in Table 1.

dients across the mixing layer and therefore larger diffusion losses. As implied by Eqs. (70) and (73), the losses of charged vanadium ions increase (i.e., become more negative) linearly with the state of charge SoC, starting at nonzero values $\Delta\tilde{\varphi}_{5,s} = -\sqrt{\gamma}\mathrm{CR} = -0.784$ and $\Delta\tilde{\varphi}_{2,s} = -1$ for $\mathrm{SoC} = 0$. Given that for $\mathrm{SoC} = 0$ there are no charged vanadium ions in the deposits, these values must be interpreted as the losses that would eventually occur after the battery starts the charging process, due to the presence of the discharged vanadium ions that have crossed to the opposite channel and are stored in the wrong deposit. For fast reactions, the losses of V^{II} ions are slightly higher than those for slow reactions, while the opposite occurs for V^V. In both cases, the slight differences grow from zero up to roughly 3% as SoC grows from 0 to 1.

Greater differences appear in the flux of total vanadium ions lost from each channel, which increases nonlinearly with SoC for fast reactions, while it remains independent of SoC for slow reactions as implied by Eqs. (74) and (75). Even thought they are of the same order of magnitude, the difference in this case grows from zero up to roughly 50% as SoC varies from 0 to 1, with the fast chemistry limit resulting in higher losses.

5.2. Same total vanadium concentration and different SoCs at both channels

As a result of the different diffusion rates of vanadium ions from the positive and negative channels, an imbalance of the state of charge of the deposits, $SoC_{45} \neq SoC_{23}$, tends to build up over time. In addition, V^{II} is known to be less stable and easily oxidized when the deposit of the negative electrolyte is not well isolated from the atmosphere [53]. Thus, the analysis of asymmetric cases is also relevant. Results in this section correspond to scenarios with the same total vanadium concentration, CR = 1, but different states of charge, $SoC_{45} \neq SoC_{23}$, in the positive and negative channels.

Fig. 5 shows contour plots of the constants C^+ and C^- defining the position of the reaction sheets Σ_{35} and Σ_{24}, the dimensionless crossover flux of charged ions V^V and V^{II} in the slow chemistry limit, $\Delta\tilde{\varphi}_{i,s}$, as well as the incremental losses between the fast and slow chemistry limits, $\Delta\tilde{\varphi}_{i,f} - \Delta\tilde{\varphi}_{i,s}$, $i = \{2, 5\}$. Also shown is the total vanadium losses from the positive channel in the fast chemistry limit, $\Delta\tilde{\varphi}_{+,f}$.

It is interesting to note that the values of C^+ and C^- are strongly dependent on the SoC of the corresponding channel (SoC_{45} and SoC_{23}, respectively) but weakly dependent on that of the opposite channel. It is also noteworthy that the reaction sheets approach the center line (i.e., C^+ and C^- tend to zero) as the SoC of the corresponding channel tends to unity and that of the opposite channel tends to zero. An *a priori* unexpected feature is the possibility of reaction sheets that penetrate into the opposite channel (see Appendix A for details). For the particular conditions considered in Fig. 5, the constant C^+ becomes negative as $SoC_{45} \to 1$ and $SoC_{23} \to 0$, indicating that the reaction sheet Σ_{35} will be displaced towards the negative channel. The isocontour $C^+ = 0$, represented with a thick red line in Fig. 5, shows conditions for which Σ_{35} is located exactly in the mid plane, $y = d^+ = 0$. By contrast, the value of C^- is always negative, meaning that the reaction sheet Σ_{24} remains always in the negative channel.

As implied by Eqs. (70) and (73), the losses of charged vanadium ions in the slow chemistry limit increase linearly with SoC_{45} and SoC_{23}. In each channel, the charged and discharged vanadium ions contribute equally to diffusion losses, but expressions (22) and (25) show that, once the effect of self-discharge reactions is taken into account, the charged ions that cross to the opposite channel contribute twice as much as the discharged ions. For general values of SoC_{45} and SoC_{23} the difference between the fluxes of charged vanadium ions lost in the fast and the slow chemistry limits are small, indicating that the rate of self-discharge reactions is irrelevant for estimating these losses. The relative changes are always below 3% and are positive (slightly less losses) for V^V and negative (slightly more losses) for V^{II}, as already observed for symmetric concentrations in the previous section. It is interesting to note that over the isocontour $C^+ = 0$ the limits of fast and slow chemistry predict the same losses for the V^V ion.

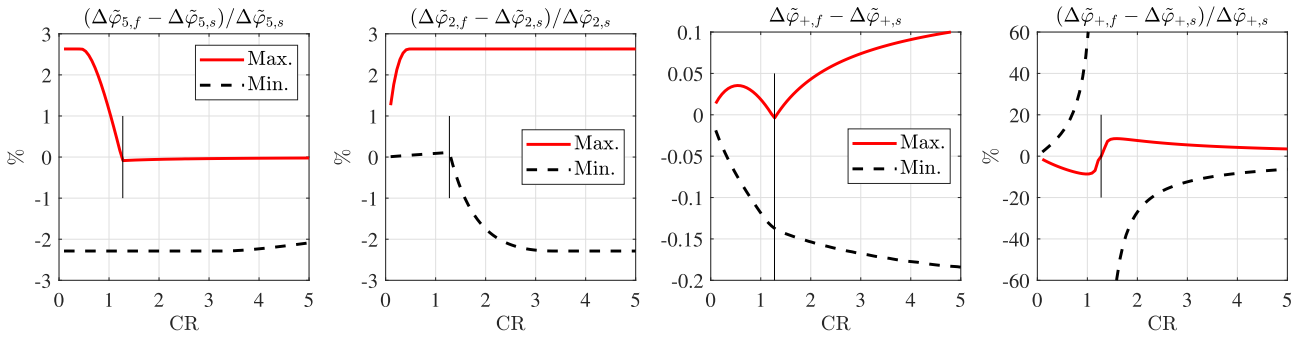

Fig. 6. Variation with CR of the maximum and minimum values of $\Delta\tilde{\varphi}_{i,f} - \Delta\tilde{\varphi}_{i,s}$ in the (SoC_{23}, SoC_{45})-plane expressed as percentage of $\Delta\tilde{\varphi}_{i,s}$ for ions V^V (left) and V^{II} (center left), and of the maximum and minimum values of $\Delta\tilde{\varphi}_{+,f} - \Delta\tilde{\varphi}_{+,s} = \Delta\tilde{\varphi}_{+,f} - (\sqrt{\gamma}CR - 1)$ in absolute value (center right) and as percentage of $\Delta\tilde{\varphi}_{+,s}$ (right). The vertical black lines correspond to $CR = 1/\sqrt{\gamma} = 1.275$. The operating parameters used for the calculations are presented in Table 1.

Something different occurs when total vanadium losses are considered. The upper right panel of Fig. 5 represents the total flux of vanadium ions lost from the positive channel for the case of fast reactions. The corresponding constant value for the limiting case of slow reactions is $\Delta\tilde{\varphi}_{+,s} = \sqrt{\gamma}\ CR - 1 = -0.2155$, marked with a thick red curve in the figure. Despite the associated losses are of the same order of magnitude in both limits, fast reactions produce an increase of up to 50% on the total vanadium lost from the positive channel, as previously noted for the case of symmetric concentrations.

5.3. Maximum and minimum losses

Fig. 5 shows that the losses of charged vanadium ions and of total vanadium ions exhibit, respectively, small and moderate differences between the slow and fast chemistry limits. The study presented in this section reports upper and lower bounds for these differences in the (SoC_{23}, SoC_{45})-plane for a wide range of concentration ratios $CR \in [0.1, 5]$. The results, shown in Fig. 6, were obtained considering all possible values of SoC_{23} and SoC_{45} and selecting only the maximum and minimum value of the variables under study.

The left and center panels show the variations with CR of the maximum and minimum differences between the losses of charged vanadium ions V^V and V^{II} in the fast and slow chemistry limits. These differences stay within ±3% when measured with those of the slow chemistry limit for all concentration ratios, confirming that the self-discharge reactions rates have a small influence in the losses of charged vanadium ions from both channels. The right panel shows the variations with CR of the maximum and minimum differences between the total flux of vanadium ions from the positive channel for fast and slow chemistry. According to Eq. (74), the total vanadium losses in the slow chemistry limit, $\Delta\tilde{\varphi}_{+,s} = \sqrt{\gamma}CR - 1$, are independent of the state of charge of the electrolytes, growing linearly with the total vanadium concentration ratio CR from -1 at $CR = 0$, changing sign at $CR = 1/\sqrt{\gamma} = 1.275$, and becoming more and more positive as CR grows above this value. In the case of fast reactions the total vanadium losses are different, with the larger relative differences occurring circa $CR = 1/\sqrt{\gamma} = 1.275$, where the slow chemistry limit predicts zero total vanadium losses. However, the absolute differences between fast and slow chemistry are still moderately small.

The parametric study presented in this section indicates that the values of the losses of charged and total vanadium ions in both channels are very similar in the limits of slow and fast self-discharge reactions, thus enabling the use of the analytical expressions (73)-(74) obtained for slow self-discharge reactions for the estimation of these loses in first approximation. Larger relative errors are expected to affect the losses of total vanadium ions, but still the slow chemistry limit may be used to get useful estimations for preliminary design purposes.

6. Generalization to three-dimensional cells

The analysis presented so far assumes the velocity of the liquid, $\vec{u} = U\vec{e}_x$, to be uniform throughout the mixing layer. This is a good approximation whenever the channel depth, $2W$, is large compared to the channel height, $2H$, because in this case the velocity at the center plane, $y = 0$, only decays from its maximum value U at distances of order $\Delta z \sim H \ll W$ from the end walls, $z = \pm W$. As a result, the variations of the axial velocity component U are negligible over most of the channel depth and the analysis presented above gives accurate results.

When the channel depth and height are of the same order, $W \sim H$, the velocity distribution at the center plane, $\vec{u} = U(z)\vec{e}_x$, is no longer uniform. This leads to a characteristic mixing layer thickness $\delta_i(z) \sim \sqrt{D_i L/U(z)}$ that varies with z, exhibiting a minimum thickness $\delta_{i,\min} \sim \sqrt{D_i L/U_{\max}}$ at the channel center, where the flow velocity reaches its maximum, $U_{\max} = U(0)$. The diffusive flux of vanadium ions crossing the center plane $y = 0$ per unit depth is also a function of z, given in first approximation by $\alpha_i(z) = c_{i,0}\sqrt{D_i U(z) L/\pi}$ for slow self-discharge reactions, a result that follows from Eq. (21).

Integrating the above expression for $\alpha_i(z)$ over the channel depth leads to the following estimate of the total flux of vanadium ions crossing the center plane

$$\alpha_i^{3D} = \int_{-W}^{W} c_{i,0}\sqrt{\frac{D_i U(z) L}{\pi}}\,\mathrm{d}z = 2W c_{i,0}\sqrt{\frac{D_i U_{\mathrm{avg}} L}{\pi}}\sqrt{\mathcal{F}(\Lambda)}\,\mathcal{I}(\Lambda) \tag{76}$$

with

$$\mathcal{F}(\Lambda) = \frac{U_{\max}}{U_{\mathrm{avg}}} \quad \text{and} \quad \mathcal{I}(\Lambda) = \frac{1}{2W}\int_{-W}^{W}\sqrt{\frac{U(z)}{U_{\max}}}\,\mathrm{d}z \tag{77}$$

where $U_{\mathrm{avg}} = Q/(4WH)$ is the average flow velocity in the channel based on the volume flow rate Q, while $\Lambda = W/H$ represents the aspect ratio of the channel cross-section, with $\Lambda \gg 1$ corresponding to the quasi two-dimensional flows considered in the previous sections with $\mathcal{F}(\Lambda) \to 3/2$ and $\mathcal{I}(\Lambda) \to 1$ as $\Lambda \to \infty$. Appendix B provides approximated expressions for $\mathcal{F}(\Lambda)$ and $\mathcal{I}(\Lambda)$ obtained from cubic polynomial fits to the exact series solution of Poiseuille's flow in rectangular cross-section channels with $\Lambda \sim 1$, for which $\mathcal{F}(\Lambda) \simeq 2$. Note that for small aspect ratios, $\Lambda \ll 1$, the velocity at the center plane $y = 0$ can be closely approximated by the parabolic profile $U(z) = U_{\max}[1 - (z/W)^2]$, in which case the asymptotic behavior $\mathcal{F}(\Lambda) \to 3/2$ and $\mathcal{I}(\Lambda) \to \pi/4$ is ob-

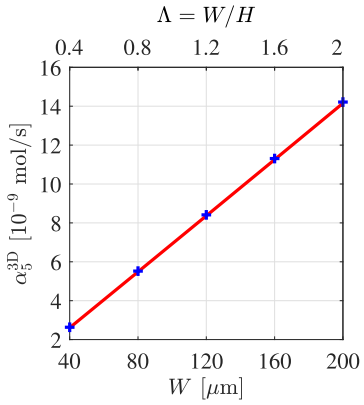

Fig. 7. Variation with the cell depth of the total flux of V^V crossing the center plane, α_5^{3D}, in the three-dimensional configuration sketched in Fig. 1 obtained numerically (symbols) and using Eq. (76) (solid line) for fixed values of the average velocity, $U_{avg} = 20$ mm/s, channel length, $L = 1$ mm, channel height, $H = 0.1$ mm, diffusion coefficient, $D_5 = 3.9 \times 10^{-10}$ m^2/s, and initial concentration, $c_{5,0} = 600$ mol/m^3.

tained as $\Lambda \to 0$. These results can be used for preliminary design purposes or order of magnitude estimates.

At $z = \pm W$, where the mixing layer enter in contact with the front and back walls, the velocity of the liquid decreases to zero due to the no-slip condition and the boundary layer approximation (6) leading to Eq. (21) for α_i does not hold. As shown in [54], the thickness of the mixing layer near the walls scales as $\delta_w \sim (D_i LW/U_{max})^{1/3}$ when the new scales for the velocity are introduced. Nevertheless, the contribution of these regions to the overall fluxes Θ_i can be neglected if $\delta_w \ll W$, which can be expressed also as $\delta_{i,min} \ll W$. On the other hand, as the mixing layer grows faster near walls, condition, $\delta_w \ll H$ must be satisfied, so that the mixing layer does not enter in contact with the electrodes. This condition can be expressed in terms of the minimum mixing layer thickness as $\delta_{i,min}/H \ll \sqrt{H/W}$.

The validity of expression (76) supplemented with the polynomial fits for $\mathcal{F}(\Lambda)$ and $\mathcal{I}(\Lambda)$ given in Eq. (91) and the coefficients given in Table 2 has been assessed against numerical simulations of rectangular cross-section channels of varying depths W in the z-direction, keeping the remaining parameters fixed. The numerical study assumes, in particular, a constant average flow velocity U_{avg}, which results in volume flow rates $Q = (4WH)U_{avg}$ that grow linearly with W. The three dimensional Navier-Stokes equations are integrated along with the convection-diffusion-reaction equations obtained by adding the second z-derivative to the diffusive term in Eq. (6) using the finite element method software COMSOL Multiphysics [50]. At the inlet section, uniform concentrations and fully developed flow velocity profiles are imposed in each subchannel. No-slip and no-flux boundary conditions are specified at the surrounding walls, while outflow boundary conditions are used at the outlet section. Special attention to the discretization of the mixing region is given in order to assure the concentration gradients are correctly resolved. For that, several numerical tests were carried out until a mesh-independent solution was finally obtained not affected by the mesh density.

The results presented in Fig. 7 show excellent agreement of the predicted flux of the vanadium ion V^V with a relative error below 1% in all cases under study. This indicates that Eq. (76), together with the piecewise polynomial fits given in Appendix B for $\mathcal{F}(\Lambda)$ and $\mathcal{I}(\Lambda)$, can be accurately used to predict the vanadium ion losses for a given cell design. Note that the analysis presented here is still valid for non-rectangular cross-section cells, such as H-shaped or trapezoidal cells, by conveniently replacing the functions $\mathcal{F}(\Lambda)$ and $\mathcal{I}(\Lambda)$ by those corresponding to Poiseuille flow in the geometry of choice.

7. Limitations of the analysis

As a final remark, this section summarizes the main limitations of the model presented in this work. These limitations could be addressed in future work to extend the validity of the model to more realistic situations:

- The mixing layer is assumed to be separated from the electrodes. For this condition to hold, it is required that the characteristic thickness of the mixing layer is small compared to the channel height, $\delta_i \sim \sqrt{D_i L/U} \ll H$. In the fast chemistry limit, the criterium changes to $d^{\pm}(L) \sim 2C^{\pm}\sqrt{D_5 L/U} \ll H$, where $d^{\pm}(L)$ represent the position of the two reaction sheets at the outlet section. As seen in Appendix A, extreme values of $C^{\pm}$ are always of order unity, so that both criteria are completely equivalent. As shown before, when three-dimensional effects are taken into account, condition $\delta_{i,min}/H \ll \sqrt{H/W}$ must also be satisfied to ensure the mixing layer near the front and back walls do not enter in contact with the electrodes.
- The densities of the two electrolytes are assumed to be equal, hence gravity effects can be ignored. Small density differences may generate a reorientation of the mixing layer [55]. As a result, the present study only holds for favourable cell orientations with the lighter electrolyte on top and the heavier on the bottom.
- The parametric studies have imposed no limitations to the inlet concentrations. Even in the fast chemistry limit, the self-discharge reaction rates can be strongly limited by the lack of reactants if the inlet concentrations are sufficiently low. Therefore, the results of the fast reaction limit are restricted to values of the SoCs and of the total vanadium concentration ratio of order unity, leaving aside extremely low values of these variables that may lead to negative values of C^+ or positive values of C^- which are not correctly accounted for in Eqs. (66)-(61).
- In the slow chemistry limit, vanadium ions of one channel may cross the mixing layer and reach the wrong deposit. From there they may be recirculated back into the cell trough the opposite channel, producing a mixed potential when entering into contact with the opposite electrode. Here it is assumed that the deposits are sufficiently large for the self-discharge reaction to take place there sooner or later. As a result, the presence of vanadium ions of the opposite electrolyte at the channel inlets is negligible.
- Transport of protons and sulphuric acid species (HSO_4^- and SO_4^{2-}) is not included in the model. Despite being present in reactions (12) and (13), the proton concentration is assumed to be in excess in first approximation. The concentration of HSO_4^- is usually very high and protons are readily produced by dissociation of the sulphuric acid, readily balancing its concentration. The concentration of sulphuric acid related species is different in each deposit due to the electroneutrality condition and the different vanadium species present in each electrolyte. The difference in concentrations generates a flux of sulphuric acid ions due to diffusion that may be calculated using the same procedure presented here.
- The migration term is neglected in Eq. (1). As all vanadium ions are positively charged, the effect of this term is that of a drift velocity in the direction of the electric field for all vanadium ions. The value of the electric field in the mixing region can be estimated from definition of the electric current

$$\nabla \Phi = -\frac{1}{\sigma}\left(\vec{i} + F\sum_i n_i D_i \nabla c_i\right). \tag{78}$$

In this study, no external current $\vec{i}$ is applied, but even if present, its effect would be negligible in first approximation as

the electric conductivity of the electrolytes is sufficiently high ($\sigma = 25$ S/m from [53]). However, due to the strong concentration gradients in the mixing region, even without an externally applied current an electric field is established that can be estimated as

$$\nabla\Phi = -\frac{\mathrm{F}\sum_i n_i D_i \nabla c_i}{\sigma}. \tag{79}$$

where the summation is extended over all ions present in the liquid. The concentration gradients across the mixing region can be estimated as $\nabla c_i \sim c_i/\delta_i$ leading to $\nabla\Phi \approx 70$ V/m at most as obtained using the values of Table 1. With this estimated values, the electric potential difference across the mixing region, of order $\Delta\Phi \sim \delta_i \nabla\Phi$, yields a non-dimensional electric potential drop $\Delta\Phi^* \sim 1.1 \times 10^{-2}$ as computed from Eq. (5). This small value justifies neglecting the migration term in Eq. (1). On top of this, the effects of the electric field will be mainly absorbed by the proton motion, as their mobility is an order of magnitude greater than that of the other ions.

8. Conclusions and remarks

The influence of the rates of the self-discharge reactions in membrane-free vanadium micro redox flow batteries is studied for the two limiting cases of slow and fast chemistry. The structure of the solution is very different in both limits. For slow reactions vanadium species mix without reaction in the cell and the resulting convection-diffusion problem is to be solved for each ion separately. The solution can be obtained in terms of error functions that describe the transversal concentration profiles of each vanadium species. On the other hand, the solution in the fast reactions limit presents two reaction fronts that travel outwards, confining a central region where only discharged ions are present and consuming the charged ions present in the bulk fluid, far from the center region. An analytical solution is obtained in terms of passive scalars free from chemical reaction terms that can be written as piecewise error functions, which requires the solution of a non-linear system of equations that can be reduced to the solution of a simple algebraic non-linear equation. Once obtained, the solution provides the position of the reaction fronts and the concentration profiles of each vanadium ion, that can be integrated at the outlet sections to estimate the losses of the different ions including also the effect of the self-discharge reactions that occur downstream the cell.

Despite having very different structures, the loss of vanadium ions is shown to be controlled by diffusion in both limits and, therefore, the scaling with the different parameters of the problem is similar in both limits. Comparing the loss of charged vanadium ions and the variations on the total vanadium concentration in each Channel for both limits it is concluded that the simple solution obtained for slow self-discharge reactions is a good approximation of the losses of charged vanadium ions (with less than 3% error) and provides a good order-of-magnitude estimation of the total vanadium ions that cross the mixing layer (with less than 50% error) regardless of the actual kinetics of the self-discharge reactions, which are yet to be described in the literature. The solutions and estimates presented here can be easily adapted to other redox couples and to help in the preliminary design of new membrane-free micro RFB architectures.

Declaration of Competing Interest

The authors declare that they have no known competing financial interests or personal relationships that could have appeared to influence the work reported in this paper.

Acknowledgements

This work has been partially funded by the Agencia Estatal de Investigación (PID2019-106740RB-I00/AEI/10.13039/501100011033), by Grant IND2019/AMB-17273 of the Comunidad de Madrid and by project MFreeB which have received funding from the European Research Council (ERC) under the European Union's Horizon 2020 research and innovation program (Grant Agreement No. 726217). S. E. Ibáñez gratefully acknowledges Dr. Rebeca Marcilla for its insightful discussions. P.A. García-Salaberri also acknowledges the support of the project PEM4ENERGY-CM-UC3M funded by the call "Programa de apoyo a la realización de proyectos interdisciplinares de I+D para jóvenes investigadores de la Universidad Carlos III de Madrid 2019–2020" under the frame of the "Convenio Plurianual Comunidad de Madrid-Universidad Carlos III de Madrid".

The solution to the set of Eqs. (54)-(59) can be reduced to the solution of a single nonlinear equation for C^+ and C^-. First, the constants A_1, A_2, B_1 and B_2 are written in terms of C^+ and C^- using Eqs. (54)-(57) to give

$$A_1 = -z_1^+\left[\frac{1+\mathrm{erf}(C^+)}{1-\mathrm{erf}(C^+)}\right], \quad A_2 = -z_2^+\left[\frac{1+\mathrm{erf}(C^-)}{1-\mathrm{erf}(C^-)}\right], \tag{80}$$

$$B_1 = -z_1^-\left[\frac{1-\mathrm{erf}(C^+)}{1+\mathrm{erf}\left(C^+/\sqrt{\gamma}\right)}\right], \quad B_2 = -z_2^-\left[\frac{1-\mathrm{erf}(C^-)}{1+\mathrm{erf}\left(C^-/\sqrt{\gamma}\right)}\right]. \tag{81}$$

Using these expressions in (58) and (59) leads to the following equation for $C^\pm$

$$F(C^\pm) = \sqrt{\gamma}\,\mathrm{CR}\,G^\pm(\mathrm{SoC}_{23}, \mathrm{SoC}_{45}) \tag{82}$$

where

$$F(C^\pm) = \left[\frac{1+\mathrm{erf}\left(C^\pm/\sqrt{\gamma}\right)}{1-\mathrm{erf}(C^\pm)}\right]\exp\left[\left(\frac{1}{\gamma}-1\right)\left(C^\pm\right)^2\right], \tag{83}$$

and

$$G^+(\mathrm{SoC}_{23}, \mathrm{SoC}_{45}) = \frac{1+\mathrm{SoC}_{23}}{\mathrm{SoC}_{45}} \in [1, \infty], \tag{84}$$

$$G^-(\mathrm{SoC}_{23}, \mathrm{SoC}_{45}) = \frac{\mathrm{SoC}_{23}}{1+\mathrm{SoC}_{45}} \in [0, 1]. \tag{85}$$

As shown in Fig. 8, the function $F(C^\pm)$ grows monotonous and smoothly with $C^\pm$. As a result, the numerical solution of Eq. (82) provides the values of $C^\pm$ in a few iterations, using, e.g., a Newton-Raphson method with $C_0^\pm = 0$ as initial guess.

It is worth noting that the values of G^+ and G^- are bounded below and above by unity, as implied by Eqs. (84) and (85). As a result, the values of C^+ and C^- are also bounded below and above by the solution $C^+_{\min} = C^-_{\max}$ of Eq. (82) obtained for $G^\pm = 1$. The minimum value of C^+ occurs for $\mathrm{SoC}_{23} = 0$ and $\mathrm{SoC}_{45} = 1$, while the maximum value of C^- occurs for $\mathrm{SoC}_{23} = 1$ and $\mathrm{SoC}_{45} = 0$. These limiting values are reached respectively in the upper-left and bottom-right corners of the C^+ and C^- subplots of Fig. 5, which show the particular case $\mathrm{CR} = 1$, for which $C^+_{\min} = C^-_{\max} = -0.09727$.

Fig. 8 also shows that as $\mathrm{CR}\sqrt{\gamma}$ becomes moderately small or large compared to unity, the limiting value $C^+_{\min} = C^-_{\max}$ grows to negative or positive values of order unity. This may result in both values of $C^+ < 0$ for $\mathrm{SoC}_{23} \to 0$ and $\mathrm{SoC}_{45} \to 1$ or values of $C^- > 0$ for $\mathrm{SoC}_{23} \to 1$ and $\mathrm{SoC}_{45} \to 0$. Under these limiting conditions, the reaction sheets Σ_{35} or Σ_{24} may be shifted respectively towards the negative or positive channels. This would invalidate the expressions for $\Delta\varphi_{i,f}$, $i = \{2, 3, 4, 5, +, -\}$ given in Eqs. (61)-(66), as they assumed that the positive and negative reaction sheets Σ_{35} and Σ_{24} were located in their corresponding channels. These limits of

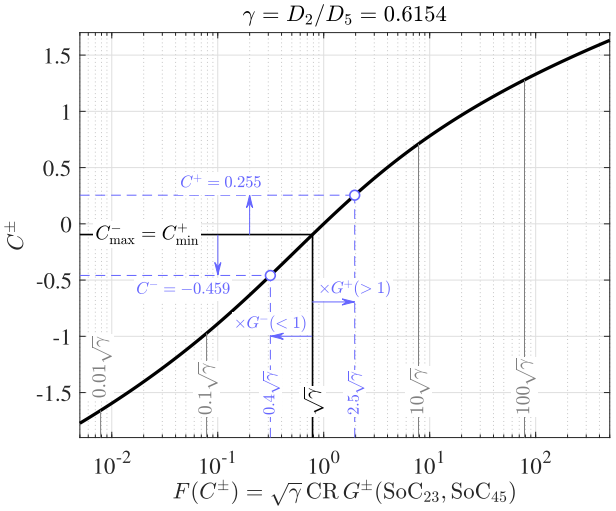

Fig. 8. Variation of $C^\pm$ with $\sqrt{\gamma}\,\mathrm{CR}\,G^\pm(\mathrm{SoC}_{23}, \mathrm{SoC}_{45})$ as predicted by Eqs. (82) and (83). Vertical straight lines provide the limiting values $C^-_{\max} = C^+_{\min}$ for different values of $\mathrm{CR} = \{0.01, 0.1, 1, 10, 100\}$ with $\gamma = D_2/D_5 = 0.6154$. Dashed blue lines illustrate the numerical application to the case of Fig. 3, corresponding to $\mathrm{CR} = 1$, $G^- = 0.4$ and $G^+ = 2.5$, with $G^\pm$ given by Eqs. (84) and (85) using $\mathrm{SoC}_{45} = \mathrm{SoC}_{45} = 2/3$. (For interpretation of the references to colour in this figure legend, the reader is referred to the web version of this article.)

highly unbalanced electrolytes are not of practical interest and will receive no further attention here.

The exact analytical solution of Poiseuille flow in a rectangular channel with walls at $\tilde{y} = y/H = \pm 1$ and $\tilde{z} = z/H = \pm\Lambda$ is given in dimensionless form by

$$\frac{U(y,z)}{P_\ell H^2/\mu} = \frac{16}{\pi^3}\sum_{n=0}^{\infty}\frac{(-1)^n}{(2n+1)^3}\left\{1 - \frac{\cosh[(2n+1)(\pi/2)\tilde{z}]}{\cosh[(2n+1)(\pi/2)\Lambda]}\right\} \cos[(2n+1)(\pi/2)\tilde{y}] \tag{86}$$

where $\Lambda = W/H$ is the aspect ratio of the channel cross section and $P_\ell = -\partial p/\partial x$ is the streamwise pressure gradient. Integration over the channel yields the average flow velocity $U_{\mathrm{avg}} = Q/(4HW)$ based on the volume flow rate, Q, as follows

$$\frac{U_{\mathrm{avg}}}{(P_\ell H^2/\mu)} = \frac{1}{3} - \frac{64}{\pi^5\Lambda}\sum_{n=0}^{\infty}\frac{\tanh[(2n+1)(\pi/2)\Lambda]}{(2n+1)^5} \tag{87}$$

Combination of the above expressions yields the maximum to average fluid velocity ratio

$$\mathcal{F}(\Lambda) = \frac{U_{\max}}{U_{\mathrm{avg}}} = \frac{U(0,0)}{U_{\mathrm{avg}}} = \frac{\frac{16}{\pi^3}\sum_{n=0}^{\infty}\frac{(-1)^n}{(2n+1)^3}\left\{1 - \frac{1}{\cosh[(2n+1)(\pi/2)\Lambda]}\right\}}{\frac{1}{3} - \frac{64}{\pi^5\Lambda}\sum_{n=0}^{\infty}\frac{\tanh[(2n+1)(\pi/2)\Lambda]}{(2n+1)^5}} \tag{88}$$

and the dimensionless velocity profile at the center plane

$$\frac{U(z)}{U_{\max}} = \frac{U(0,z)}{U(0,0)} = \frac{\sum_{n=0}^{\infty}\frac{(-1)^n}{(2n+1)^3}\left\{1 - \frac{\cosh[(2n+1)(\pi/2)\tilde{z}]}{\cosh[(2n+1)(\pi/2)\Lambda]}\right\}}{\sum_{n=0}^{\infty}\frac{(-1)^n}{(2n+1)^3}\left\{1 - \frac{1}{\cosh[(2n+1)(\pi/2)\Lambda]}\right\}} \equiv \tilde{u}(\tilde{z};\Lambda) \tag{89}$$

required to evaluate the integral

$$\mathcal{I}(\Lambda) = \frac{1}{2W}\int_{-W}^{W}\sqrt{\frac{U(z)}{U_{\max}}}\,\mathrm{d}z = \frac{1}{2\Lambda}\int_{-\Lambda}^{\Lambda}\sqrt{\tilde{u}(\tilde{z};\Lambda)}\,\mathrm{d}\tilde{z} \tag{90}$$

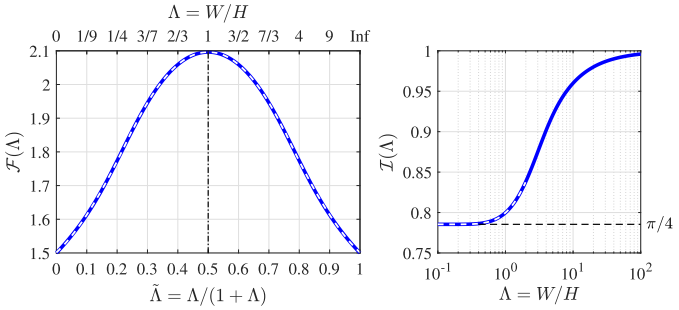

Fig. 9. Functions $\mathcal{F}(\Lambda)$ and $\mathcal{I}(\Lambda)$ (solid lines) represented along with the polynomial fits given in Eq. (91) using the coefficients given in Table 2 (white dashed lines). The relative error of the fits remains always below 2×10^{-3}. Note the symmetry of $\mathcal{F}(\Lambda)$ with respect to $\tilde{\Lambda} = 0.5$. The asymptotic result $\mathcal{I}(\Lambda) \to \pi/4$ as $\Lambda \to 0$ corresponds to a planar Poiseuille flow with parabolic velocity profile, and can be used with less than 2% error in the range $0 \le \Lambda \lesssim 1$.

Table 2
Coefficients to be used in the polynomial fits for $\mathcal{F}(\Lambda)$ and $\mathcal{I}(\Lambda)$ given in equation (91), with indication of the parametric range of validity and the maximum relative error in that range.

f_3	f_2	f_1	f_0	range	rel. error
−2.4515	3.1157	0.8313	1.5015	$0 \le \tilde{\Lambda} \le 0.25$	$< 2 \times 10^{-3}$
−0.8174	−2.8182	3.4047	1.2003	$0.25 < \tilde{\Lambda} \le 0.5$	$< 1 \times 10^{-3}$
i_3	i_2	i_1	i_0	range	rel. error
0	0	0	$\pi/4$	$0 \le \Lambda \le 0.2$	$< 2 \times 10^{-5}$
-0.0063	0.0317	-0.0122	0.7865	$0.2 < \Lambda \le 2$	$< 1 \times 10^{-4}$

The above expressions enable the numerical computation of the functions $\mathcal{F}(\Lambda)$ and $\mathcal{I}(\Lambda)$, shown in Fig. 9 along with the piecewise cubic fits

$$\begin{aligned}\mathcal{F}(\Lambda) &= f_3\tilde{\Lambda}^3 + f_2\tilde{\Lambda}^2 + f_1\tilde{\Lambda} + f_0 \\ \mathcal{I}(\Lambda) &= i_3\Lambda^3 + i_2\Lambda^2 + i_1\Lambda + i_0\end{aligned} \tag{91}$$

where the expression for $\mathcal{F}(\Lambda)$ is written in terms of

$$\tilde{\Lambda} = \begin{cases} \Lambda/(\Lambda+1) & \text{for} \quad 0 \le \Lambda \le 1 \\ 1/(\Lambda+1) & \text{for} \quad 1 \le \Lambda < \infty \end{cases} \tag{92}$$

to exploit the symmetry $\Lambda \leftrightarrow \Lambda^{-1}$, and the coefficients f_i and i_i are given in Table 2. The above expressions yield small relative errors and can be used for fast and accurate evaluations of Θ_i from Eq. (76), leading to the results shown in Fig. 7.

References

[1] M.Y. Suberu, M.W. Mustafa, N. Bashir, Energy storage systems for renewable energy power sector integration and mitigation of intermittency, Renewable Sustainable Energy Rev. 35 (2014) 499–514.
[2] J.P. Barton, D.G. Infield, Energy storage and its use with intermittent renewable energy, IEEE Trans. Energy Convers. 19 (2) (2004) 441–448.
[3] M.L. Perry, A.Z. Weber, Advanced redox-flow batteries: a perspective, J Electrochem Soc 163 (1) (2016) A5064–A5067.
[4] J. Marschewski, P. Ruch, N. Ebejer, O.H. Kanan, G. Lhermitte, Q. Cabrol, B. Michel, D. Poulikakos, On the mass transfer performance enhancement of membraneless redox flow cells with mixing promoters, Int J Heat Mass Transf 106 (2017) 884–894.
[5] M. Park, J. Ryu, W. Wang, J. Cho, Material design and engineering of next-generation flow-battery technologies, Nat. Rev. Mater. 2 (1) (2016) 1–18.
[6] A.M. Pezeshki, J.T. Clement, G.M. Veith, T.A. Zawodzinski, M.M. Mench, High performance electrodes in vanadium redox flow batteries through oxygen-enriched thermal activation, J Power Sources 294 (2015) 333–338.
[7] J.Z. Chen, W.Y. Liao, W.Y. Hsieh, C.C. Hsu, Y.S. Chen, All-vanadium redox flow batteries with graphite felt electrodes treated by atmospheric pressure plasma jets, J Power Sources 274 (2015) 894–898.
[8] L. Wei, T.S. Zhao, G. Zhao, L. An, L. Zeng, A high-performance carbon nanoparticle-decorated graphite felt electrode for vanadium redox flow batteries, Appl Energy 176 (2016) 74–79.
[9] M.A. Goulet, O.A. Ibrahim, W.H. Kim, E. Kjeang, Maximizing the power density of aqueous electrochemical flow cells with in operando deposition, J Power Sources 339 (2017) 80–85.
[10] M. Skyllas-Kazacos, M. Rychcik, R.G. Robins, A.G. Fane, M.A. Green, New all–vanadium redox flow cell, J Electrochem Soc 133 (1986) 1057.

[11] M. Park, J. Ryu, J. Cho, Nanostructured electrocatalysts for all-vanadium redox flow batteries, Chemistry-An Asian Journal 10 (10) (2015) 2096–2110.
[12] P.A. García-Salaberri, T.C. Gokoglan, S.E. Ibáñez, E. Agar, M. Vera, Modeling the effect of channel tapering on the pressure drop and flow distribution characteristics of interdigitated flow fields in redox flow batteries, Processes 8 (7) (2020) 775.
[13] E. Kjeang, N. Djilali, D. Sinton, Microfluidic fuel cells: a review, J Power Sources 186 (2) (2009) 353–369.
[14] J.P. Esquivel, P. Alday, O.A. Ibrahim, B. Fernández, E. Kjeang, N. Sabaté, A metal-free and biotically degradable battery for portable single-use applications, Adv Energy Mater 7 (18) (2017) 1700275.
[15] R. Ferrigno, A.D. Stroock, T.D. Clark, M. Mayer, G.M. Whitesides, Membraneless vanadium redox fuel cell using laminar flow, J. Am. Chem. Soc. 124 (44) (2002) 12930–12931.
[16] E.R. Choban, L.J. Markoski, A. Wieckowski, P.J. Kenis, Microfluidic fuel cell based on laminar flow, J Power Sources 128 (1) (2004) 54–60.
[17] E. Kjeang, J. McKechnie, D. Sinton, N. Djilali, Planar and three-dimensional microfluidic fuel cell architectures based on graphite rod electrodes, J Power Sources 168 (2) (2007) 379–390.
[18] E. Kjeang, R. Michel, D.A. Harrington, N. Djilali, D. Sinton, A microfluidic fuel cell with flow-through porous electrodes, J. Am. Chem. Soc. 130 (12) (2008) 4000–4006.
[19] J.W. Lee, M.A. Goulet, E. Kjeang, Microfluidic redox battery, Lab Chip 13 (13) (2013) 2504–2507.
[20] M.A. Goulet, O.A. Ibrahim, W.H. Kim, E. Kjeang, Maximizing the power density of aqueous electrochemical flow cells with in operando deposition, J Power Sources 339 (2017) 80–85.
[21] P. Navalpotro, J. Palma, M. Anderson, R. Marcilla, A membrane-free redox flow battery with two immiscible redox electrolytes, Angewandte Chemie 129 (41) (2017) 12634–12639.
[22] K. Oh, M. Moazzam, G. Gwak, H. Ju, Water crossover phenomena in all-vanadium redox flow batteries, Electrochim. Acta 297 (2019) 101–111.
[23] S.A.M. Shaegh, N.T. Nguyen, S.H. Chan, A review on membraneless laminar flow-based fuel cells, Int J Hydrogen Energy 36 (9) (2011) 5675–5694.
[24] J. Marschewski, P. Ruch, N. Ebejer, O.H. Kanan, G. Lhermitte, Q. Cabrol, D. Poulikakos, On the mass transfer performance enhancement of membraneless redox flow cells with mixing promoters, Int J Heat Mass Transf 106 (2017) 884–894.
[25] K.J. Kim, M.S. Park, Y.J. Kim, J.H. Kim, S.X. Dou, M. Skyllas-Kazacos, A technology review of electrodes and reaction mechanisms in vanadium redox flow batteries, Journal of materials chemistry a 3 (33) (2015) 16913–16933.
[26] N. Roznyatovskaya, J. Noack, K. Pinkwart, J. Tübke, Aspects of electron transfer processes in vanadium redox-flow batteries, Curr. Opin. Electrochem. 19 (2020) 42–48 In press, doi:10.1016/j.coelec.2019.10.003.
[27] A.M. Limaye, A.P. Willard, Modeling interfacial electron transfer in the double layer: the interplay between electrode coupling and electrostatic driving, J. Phys. Chem. C 124 (2) (2020) 1352–1361 In press, doi:10.1021/acs.jpcc.9b08438.
[28] J. Marschewski, S. Jung, P. Ruch, N. Prasad, S. Mazzotti, B. Michel, D. Poulikakos, Mixing with herringbone-inspired microstructures: overcoming the diffusion limit in co-laminar microfluidic devices, Lab Chip 15 (8) (2015) 1923–1933.
[29] M.R. Holl, P. Galambos, F.K. Forster, J.P. Brody, M.A. Afromowitz, P. Yager, Optimal Design of a microfabricated diffusion-based extraction device, in: Proceedings of 1996 ASME Meeting ASME DSC, volume 59, 1996, pp. 189–195.
[30] H.B. Park, D.H. Ahmed, K.H. Lee, H.J. Sung, An h-shaped design for membraneless micro fuel cells, Electrochim. Acta 54 (18) (2009) 4416–4425.
[31] A. Tang, J. Bao, M. Skyllas-Kazacos, Dynamic modelling of the effects of ion diffusion and side reactions on the capacity loss for vanadium redox flow battery, J Power Sources 196 (24) (2011) 10737–10747.
[32] M. Skyllas-Kazacos, L. Goh, Modeling of vanadium ion diffusion across the ion exchange membrane in the vanadium redox battery, J Memb Sci 399 (2012) 43–48.
[33] A. Bazylak, D. Sinton, N. Djilali, Improved fuel utilization in microfluidic fuel cells: a computational study, J Power Sources 143 (1–2) (2005) 57–66.
[34] D. Krishnamurthy, E.O. Johansson, J.W. Lee, E. Kjeang, Computational modeling of microfluidic fuel cells with flow-through porous electrodes, J Power Sources 196 (23) (2011) 10019–10031.
[35] K.M. Lisboa, R.M. Cotta, On the mass transport in membraneless flow batteries with flow-by configuration, Int J Heat Mass Transf 122 (2018) 954–966.
[36] K.M. Lisboa, R.M. Cotta, Analysis of the mass transport in corrugated membraneless flow batteries, Appl Math Model 77 (2020) 1512–1530.
[37] M.A. Goulet, E. Kjeang, Reactant recirculation in electrochemical co-laminar flow cells, Electrochim. Acta 140 (2014) 217–224.
[38] M.A. Goulet, E. Kjeang, Co-laminar flow cells for electrochemical energy conversion, J Power Sources 260 (2014) 186–196.
[39] Z. Jiang, K. Klyukin, K. Miller, V. Alexandrov, Mechanistic theoretical investigation of self-discharge reactions in a vanadium redox flow battery, The Journal of Physical Chemistry B 123 (2019) 3976–3983.
[40] C. Suna, J. Chena, H. Zhanga, Q. Luoa, Investigations on transfer of water and vanadium ions across nafion membrane in an operating vanadium redox flow battery, J Power Sources 195 (2010) 890–897.
[41] K.W. Knehr, E. Agar, C.R. Dennison, A.R. Kalidindi, E.C. Kumbur, A transient vanadium flow battery model incorporating vanadium crossover and water transport through the membrane, J Electrochem Soc 159 (9) (2012) A1446.
[42] A.A. Shah, M.J. Watt-Smith, F.C. Walsh, A dynamic performance model for redox-flow batteries involving soluble species, Electrochim. Acta 53 (2008) 8087–8100.
[43] S.P. Burke, T.E.W. Schumann, Diffusion flames, Industrial & Engineering Chemistry 20 (10) (1928) 998–1004.
[44] A. Linán, M. Vera, A.L. Sánchez, Ignition, liftoff, and extinction of gaseous diffusion flames, Annu Rev Fluid Mech 47 (2015) 293–314.
[45] V.A. Shvab, The relationship between the temperature and velocity fields in a gaseous Flame, in: G.F. Knorre (Ed.), Research on Combustion Processes in Natural Fuel, Moscow: Gosenergoizdat, 1948, pp. 231–248.
[46] Y.B. Zel'dovich, Teorii gorenia neperemeshannykh gazov, Zhurnal Tekhnicheskoi Fiziki 19 (10) (1949) 1199–1210.
[47] A. Linán, The structure of diffusion flames, in: M. Onofri, A. Tesev (Eds.), Fluid Dynamical Aspects of Combustion Theory, Harlow, UK: Longman Sci. Tech., 1991, pp. 11–29.
[48] A. Linán, Diffusion-controlled Combustion, in: H. Aref, J.W. Phillips (Eds.), Mechanics for a New Millennium, Dordrecht: Kluwer Acad, 2001, pp. 487–502.
[49] T. Yamamura, N. Watanabe, T. Yano, Y. Shiokawa, Electron-transfer kinetics of Np^{3+}/Np^{4+}, NpO_2^+/NpO_2^{2+}, V^{2+}/V^{3+}, and VO^{2+}/VO_2^+ at carbon electrodes, J Electrochem Soc 152 (2005) A830–A836.
[50] COMSOL Multiphysics R v. 5.4. Available online: https://www.comsol.com (accessed on 9 October 2019).
[51] A. Liñán, On the internal structure of laminar diffusion flames, Tech. rep. osr/eoar tn 62-24, INTA, Madrid, 1961.
[52] A. Liñán, On the structure of laminar diffusion flames, Calif. Inst. Technol., Pasadena, 1963 Aeronaut. eng. thesis.
[53] M. Skyllas-Kazacos, L. Cao, M. Kazacos, N. Kausar, A. Mousa, Vanadium electrolyte studies for the vanadium redox battery-a review, ChemSusChem 9 (13) (2016) 1521–1543.
[54] R.F. Ismagilov, A.D. Stroock, P.J.A. Kenis, G. Whitesides, H.A. Stone, Experimental and theoretical scaling laws for transverse diffusive broadening in two-phase laminar flows in microchannels, Appl Phys Lett 76 (2000) 2376.
[55] J. Xuan, M.K.H. Leung, D.Y.C. Leung, H. Wang, Towards orientation-independent performance of membraneless microfluidic fuel cell: understanding the gravity effects, Appl Energy 90 (2012) 80–86.